Review

Daniel P. Otto and Melgardt M. de Villiers*

Why is the nanoscale special (or not)? Fundamental properties and how it relates to the design of nano-enabled drug delivery systems

Abstract: Nanoscience studies describe natural phenomena at the submicron scale. Below a critical nanoscale limit, the physical, chemical, and biological properties of materials show a marked departure in their behavior compared to the bulk. At the nanoscale, energy conversion is dominated by phonons, whereas at larger scales, electrons determine the process. The surface-to-volume ratio at the nanoscale is immense, and interfacial interactions are markedly more important than at the macroscopic level, where the majority of the material is shielded from the surface. These properties render the nanoparticles to be significantly different from their larger counterparts. Nano-enabled drug delivery systems have resulted from multidisciplinary cooperation aimed at improving drug delivery. Significant improvements in the thermodynamic and delivery properties are seen due to nanotechnology. Hybrid nanodelivery systems, i.e., membranes with nanopores that can gate stimuli-responsive drug release could be a future development. Nanotechnology will improve current drug delivery and create novel future delivery systems. The fundamental properties and challenges of nanodelivery systems are discussed in this review.

Keywords: nano-enabled drug delivery; nanoparticle; nanotechnology; physicochemical properties.

***Corresponding author: Melgardt M. de Villiers,** School of Pharmacy, University of Wisconsin-Madison, 777 Highland Avenue, Madison, WI 53705-2222, USA,
e-mail: mmdevilliers@pharmacy.wisc.edu
Daniel P. Otto: Catalysis and Synthesis Research Group, Chemical Resource Beneficiation Research Focus Area, Faculty of Natural Sciences, North-West University, Potchefstroom 2520, South Africa

1 Introduction to nanoscience and nanotechnology

Nanoscience can be defined as the activity aimed at the understanding of natural phenomena at a nanoscale level and nanotechnology as the novel and practical applications of this scientific knowledge [1]. Nanotechnology investigates and manipulates materials and phenomena where at least one length scale of a particle is below 100 nm as defined by the US National Nanotechnology Initiative [2]. The examples of the nanoparticles that are investigated for their drug delivery potential include metal oxides, gold and silver nanoparticles, carbon nanotubes (CNTs), dendrimers and fullerenes, liposomes and polymeric nanoparticles comprising of (bio-)polymers, modified viral carriers, and many more [3].

Although nanotechnology is not the magic bullet to all the health-related challenges, several new applications and solutions will be found that were otherwise obscured [3]. Some of the drug delivery research and development targets that were set by the NNI for 2015 are the nanoscale synthesis and manufacturing of pharmaceuticals and the treatment of cancer using nanotechnology with no mortality or toxicity [4].

Therefore, drug delivery should focus on nanotechnology, which provides a set of tools that can be utilized to mimic, monitor, and influence biological processes [5]. The versatility of nanoparticles is attributed to their size as they are significantly smaller than the 10–20 μm size of cells. However, most nanoparticles exhibit the same size as large biomolecules such as enzymes and receptors, which enables their interaction [6]. Another major advantage of nanodelivery systems is their ability to transverse biological barriers in a noninvasive way. The nanoparticles can enter most cells if they are smaller than 50 nm, while those smaller than 20 nm can exit the normal blood capillaries [7]. The tumor capillaries are usually more permeable than the healthy vessels and particles ranging at 100–1000 nm diffuse selectively into the tumor [4]. Clearly, noninvasive delivery at the nanoscale has the potential to improve the drug delivery systems and enhance the choice of the administration route. This is significant as 95% of all the new potential therapeutics demonstrates poor pharmacokinetics and bioavailability properties and, here, nanotechnology can be of great help [8].

A further valuable property of the nanoparticles is their sensing capability. A nanodelivery system could be functionalized with a suitable tracer or present size-related

properties that can be monitored *in vivo* to determine if it has reached its target. This could be an early indicator of the success or failure of a targeted drug delivery system and could shorten trials and regulatory trails [9].

Why is the nanoscale special? In the following discussions, the answers to this question will be revealed. Nanotechnology, therefore, nano-enabled drug delivery, relies on a multidisciplinary approach and echoes the original thoughts of Feynman in which he expressed that the problems of chemistry and biology could be better investigated if one could observe and manipulate at the atomic level [10]. Figure 1 shows the size scale of differently sized objects to indicate the relative size of the nanoscale.

2 The fundamental properties of nanomaterials

The deviation in the behavior of the micro- and nanoparticles from the normally observable macroscopic world forms the essence of the interest in nanoparticles. Phenomena that are considered negligible at the macroscopic level become significant at the nanoscale (10^{-9} m). At the microscopic scale (10^{-6} m), the surface tension effects outplay the gravity and particle size approaches with the same size scale as that of typical transport phenomena such as mean free paths between vibrating particles. At the nanoscopic scale, the thermodynamic behavior deviates significantly from the observable macroscopic world. The number of surface atoms in relation to the total number of bulk atoms cannot be ignored, and unique effects appear [11].

3 Surface-to-volume ratio

The surface-to-volume ratio of nanomaterials is immense compared to their macroscopic counterparts, resulting in different properties at the nanoscale. The majority of ions, molecules, or other building blocks appear on the surface for nanoparticles. The surface of a sphere scales

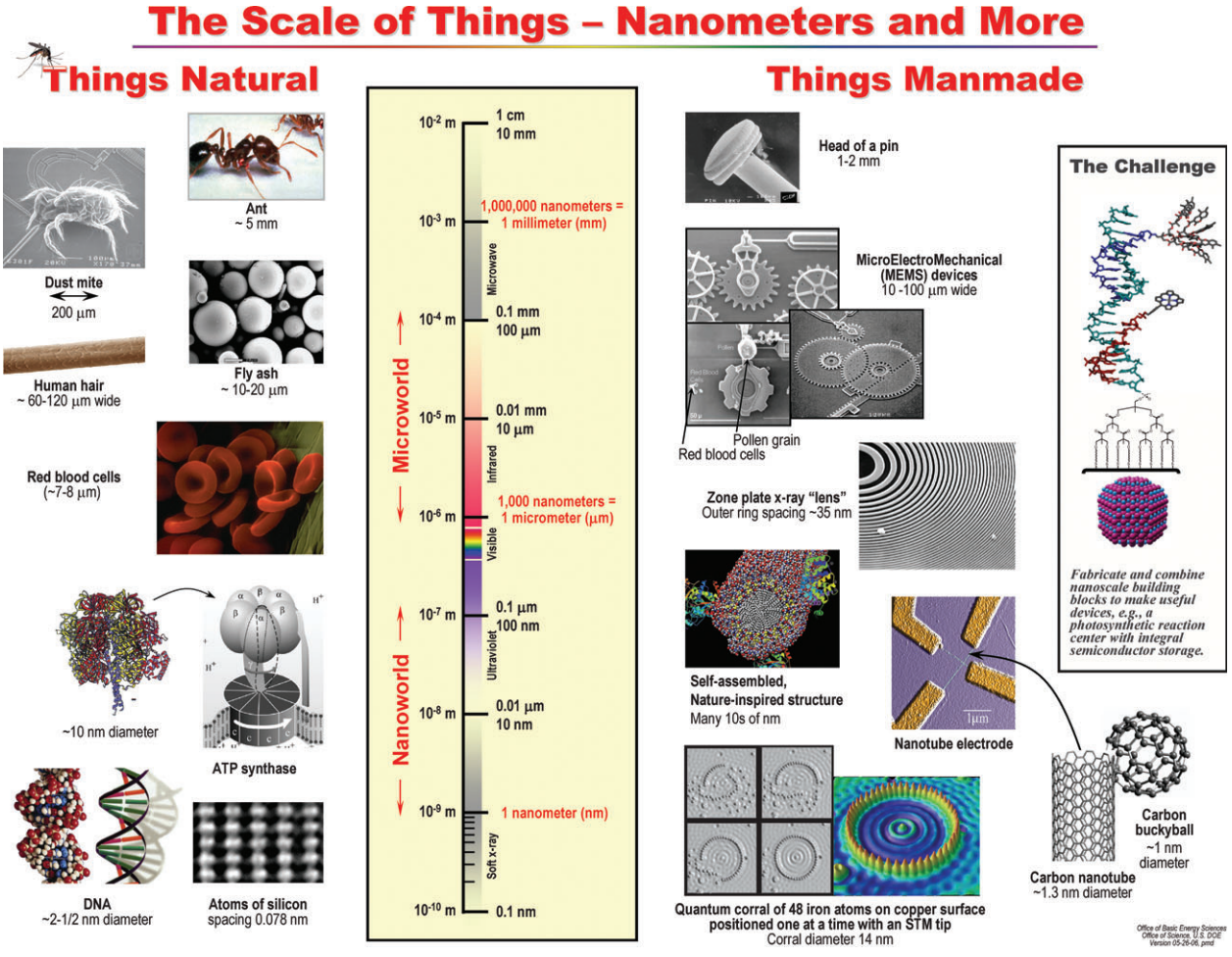

Figure 1 The relative size scale of macro-, micro-, and nanoscopic objects (reproduced with permission, US Department of Energy).

with its radius, r, and its volume scales with r^3. Thus, the surface-to-volume ratio is inversely proportional to the size. This surface dispersion is also known as the coordination number, <*NN*>, and describes the number of the nearest neighboring atoms or molecules in proximity to any single building block on the surface or bulk. The particles with significant fractions of surface atoms, *N*, have a low <*NN*>. For infinitely large clusters, the coordination number extrapolates to 12 and resembles the bulk of the material. Generally, the surface atoms of small particles are, therefore, less coordinated compared to the larger particles and show a lower cohesion. The small clusters also behave more like molecules or pseudoatoms than like a macroscopic material [12].

4 Quantum effects

The electronic structure found in the small particles is generally very discrete and not overlapping as is the case with the bulk material phases. This is due to the confinement of the electromagnetic wavefunctions to certain physical dimensions of the nanoparticles [13], an effect that is limited to the nanoscale [14].

The thermal, optical, and conductive properties of materials arise from the discrete vibration of the nearest neighbors, known as phonons. The order in a lattice of the nearest neighbors is momentarily disturbed as phonons vibrate like waves from one point to the next. The phonons are quantized or discrete, and only certain vibration frequencies are allowed. This is analogous to the term photon, referring to the emission of electrons in the form of light energy, also in discrete units of energy or quanta. Phonons are responsible for heat transfer, optical effects, and the acoustic properties observed in materials and dominate energy transfer at the nanoscale. Owing to the confinement at the nanoscale, the phonons impart different properties to the nanomaterials compared to their macroscopic, unconfined counterparts [15–17].

5 Conductive properties

Conductive polymers comprise of carbon chains in which single, sigma (σ) and double bonds alternate, forming a conjugated, sp^2-hybridized molecular orbital system that houses valence electrons. The σ bonds strongly localize valence electrons; however, the double bonds arise from accommodating additional electrons in π orbitals, which show delocalization. In cases where adjacent π orbitals overlap sufficiently, the electrons can be transferred between orbitals if a vacancy exists to accommodate the electron. In the π-conjugated chain, the potential exists for the complete molecular orbital to accommodate this electron migration along the whole chain length; however, this does not guarantee conductivity on the macroscopic scale. The conductivity is still localized inside the conjugated chain and, therefore, only semiconductive, as the overlap between conductive chains is not guaranteed to ensure a long-range conduction [18].

A dopant, such as a metal atom, is often required to connect the various conjugated chains to induce conductivity over various chains. The metal ion or dopant has additional electrons that can migrate between conductive polymer chains, and these electrons are even more delocalized in the *d* orbitals. The dopants, therefore, aid the formation of orbital "holes" in which electrons can be housed or through which the electrons can be transferred. Figure 2 illustrates the effect of molecular orbital overlap and conductivity.

Oxidation reactions induce electrons into the conductive chain, which destabilizes the chain structure [20]. The dopant coordinates, and therefore stabilizes, the conductive polymer chains to ensure a sufficient orbital overlap to induce the long-range conductive properties in the polymeric material. CNTs are very efficient dopants and enhanced the conductivity of several conductive polymer matrices at low percolation thresholds of <0.1% wt. [21]. In turn, CNTs show an insulation-to-conduction percolation threshold for several metallic fillers such as platinum and silver at doping levels of 10–20%. However, the composite material packing efficiency, surface roughness, and chemical degradations largely determines the magnitude of conductivity and might not benefit from nanoscale dimensions [22]. Recovery from mechanical stress could also influence the conductivity of the material as this will determine the recurrence of orbital overlap [23].

The conductivity of a material is described in Equation (1) [24]:

$$\sigma = ne\mu \tag{1}$$

where σ is the electrical conductivity, n is the number of charge carriers per unit volume (double bonds), e is the charge that the electron transports, and μ is the mobility or velocity at which the charge is conducted.

From Equation (1) it has now become apparent that the conduction of the charge is proportional to the number of charge conductors, n. A single molecule with only one double bond is, therefore, insulating as n=1 (μ=0). The complex structures of the molecular orbitals

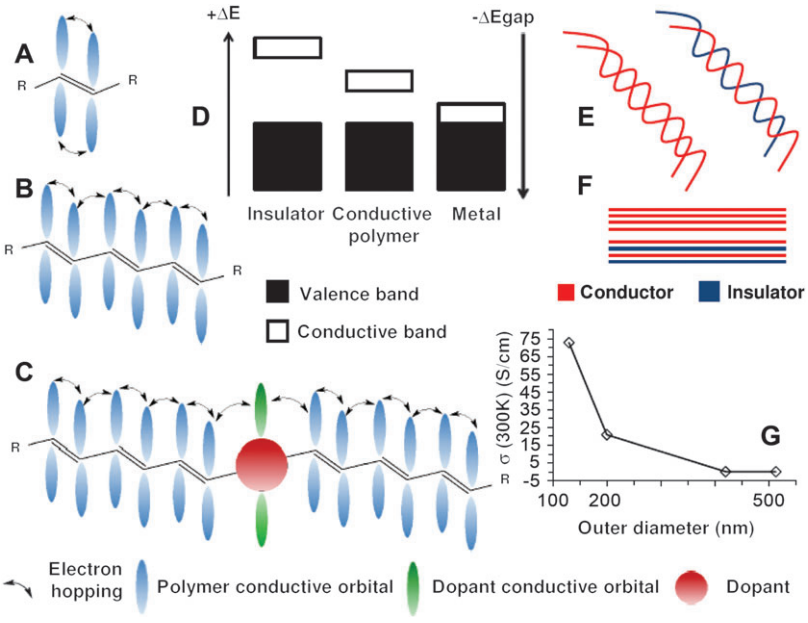

Figure 2 A depiction of the conductivity of materials for (A) a single molecule with a single double bond (N=1), (B) a molecule with several double bonds (N=3), (C) a coordinating dopant that links n conjugated chains with several double bonds (N>>1). In (D) the energy gap decreases and the probability of conductivity becomes large as N>>1. (E) and (F) indicate some extremes of geometry and the combination of conductors and insulators. The anisotropy of the conduction is significantly affected by contact points, separation distances, geometry (straight or wavy) and (G) dimensions of the conducting material [19]. [Reproduced with permission, copyright (2005) by The American Physical Society.]

of metals result in the extensive electron delocalization of the electrons between different neighboring atoms, and n assumes very large values and, therefore, metals are extremely good conductors ($\mu \rightarrow \infty$). The conductive polymers have a semiconductivity that can be modified with dopants or changes in the interchain distances, therefore, conductive ability.

A critical requirement for conduction is, therefore, the promotion of electrons to a conductive state rather than the localized state. The ease by which this promotion can be induced is characterized by an energy value or band gap and is defined as the energy gap between the valence and conductive band that can accommodate the electron [25]. Clearly, in insulators, this gap is very large, and in metals, this gap is virtually nonexistent. This energy gap is described in an oversimplified form by Equation (2) [25]:

$$\Delta E_{gap} = E_{conductive} - E_{valence} \approx \frac{h^2}{8md^2} \bullet \frac{1}{N} \qquad (2)$$

where E denotes energy, ΔE_{gap} indicates the energy gap between the conductive ($E_{conductive}$) and valence electron band ($E_{valence}$), d describes the distance separating the atoms, N describes the number of conductors aligned in a row, and m gives the mass of the electron.

From Equation (2), it is seen that as the polymer chain length, N, increases, the energy gap will approach zero, and the conduction will become more probable as $1/N \rightarrow 0$. The dopant is, thus, critical to link n chains of length N or to avoid sp^3-hybridized insulating impurities [26]. The concentration of a conductive polymer in a composite material also affects the probability of aligning n units of polymer as was illustrated for an iron oxide-pyrrole nanocomposite at the polymer percolation threshold concentration [27].

An important property in a conducting material of conjugate bonds is its three-dimensional structure in which the alignment of the conductors can, therefore, also assume these dimensions. However, nanotechnology can manipulate the structure of the conducting material. If the material was fabricated to be nanowires, the width and height becomes negligible ($N_{width}=N_{height}=1$) in relation to the length ($N_{length}>>N_{width}=N_{height}$), then, the conductivity is possible in only one direction or anisotropic ($\sigma_{total} \sim \sigma_{length}$). By decreasing the radius, the conductivity for single PPy or PANI nanotubes at a given length increases severalfold due to optimal alignment of the conductors in one direction [19, 28]. The insulation of the nanowires by increasing the perpendicular separation distance (d) between the chains can ensure that the conduction through several conducting chains is possible

in only one direction rather than between the chains. A controlled nanoarchitecture in a porous material can, therefore, be more conductive than an amorphous or bulk structure in which *d* is not well controlled or contact is localized [28, 29]. Indeed, it has been shown that CNTs will show more contact points if they were wavy compared to straight tubes. Owing to this contact, a degree of anisotropic conductivity is lost, and a lower overall conductivity is seen for the wavy tubes [30]. The insulation of CNTs by coating them with an insulating polymer could preserve the order between the nanotubes and significantly enhance the electrical conductivity of the nanocomposites [31]. Therefore, the insulation of CNTs provide a sufficient length of aligned conductors with a proportional scaling of conductivity [32] as was predicted by Equation (2). Figure 2 depicts the energy gap and the relation to the conductivity of the materials.

In the following sections of this review, nanopores will be discussed to a greater extent. However, the use of conductive polymers to create a nanoporous carrier for drugs is one of the applications of this aspect of nanotechnology. The conductive polymer conveys the attractive properties of mechanical, chemical, and physical properties of the polymers as well as the electrical conductivity to a drug delivery system. Apart from the nanoscale properties of the carrier, it can now also experience local or nanoscale electrical conductivity, which could serve as a therapeutic or stimuli-responsive release vehicle.

Owing to the conductivity susceptibility at the nanostructured level, very low current could be used to effectively produce the release stimulus. Other stimuli such as light can be used to induce current, and due to the immense surface-to-volume ratio, electrical conductivity can appear at the nanoscale, which will otherwise be impossible at the macroscopic scale. Light is a source of photons, which could promote the highest occupied molecular orbital (HOMO)-lowest unoccupied molecular orbital (LUMO) excitation and induce electrical current. It is also intuitive to assume that heat will also affect the electrical conductivity due to the effect of the phonons on the conductive orbital overlap [24]. In turn, the heat phonons would also influence the optical properties of the conduction bands, and shifts in the light absorption spectra are observed. Other factors that will influence the conductivity and insulation properties are variation of the dopant size, carbonation, and the degree of crystallinity, which affects the degree of conductive orbital overlap [33].

6 Conductive polymer nanotechnology in drug delivery

Several biomedical applications have been developed for conductive polymers and poly(pyrrole) (PPy) [34] and poly(aniline) (PANI) are the most commonly used for biological applications [35]. The third most commonly utilized biomedical conductive polymer of note is poly(3,4-ethylenedioxythiophene) (PEDOT) [36].

PPy was combined with dexamethasone phosphate as a dopant in an electrically conductive delivery device. When PPy oxidizes during the application of current, it assumes a polycationic charge, and the anionic dexamethasone phosphate is deposited on the polymer backbone. By the application of current with alternating bursts of positive and negative potential, the PPy switches between the oxidized and reduced states, i.e., between positive and neutral states. If the PPy is reduced, it releases the drug. As the potential switches again, the drug release ceases, creating a controlled delivery device [37].

Another conductive polymer, PEDOT is a popular biomedical material for neural applications. In various combinations, PEDOT and poly(D,L-lactide-*co*-glycolide) (PLGA) or poly(L-lactide) (PLLA) nanocomposites were manufactured and loaded with dexamethasone. The release of the drug could be modified according to the nanocarrier composition and responded precisely to an electrical stimulus to release the drug [38].

Owing to the high porosity of a nanoporous PPy film compared to a nonporous PPy film, the release capacity of fluorescein was nine times higher from the porous structure under electrical stimulation [39].

Several applications of conductive polymers rely on the surface adsorption of the drug or dopant and the subsequent release from the surface. However, dexamethasone was incorporated into the PPy walls of the nanotubes. The surface and lumina of the nanotubes can, therefore, contribute to control the release of the drug [39].

7 Optical properties of nanoparticles

The energy gap between HOMO and LUMO also determines the response of the phonons and electrons to light. By considering the lowest unoccupied energy state of the electronic system of a macroscopic material, the Fermi

energy, E_f, could be incorporated to describe the energy gap (Equation 3) [12]:

$$\delta = 4E_f/3n \quad (3)$$

where n is representing the number of valence electrons in the nanosystems. In the case where the thermal energy of the systems exceeds the energy gap, they will behave conductively, and if not, they will behave like insulators or like cases where valence electrons are localized. This change is especially prevalent in small systems at the nanoscale due to the physical distance and geometry effects on the orbital overlap distances [12].

The differences in optical properties are also noted for the nanosystems that are observed as luminescence and size-dependent color changes of certain metallic nanoparticles due to phonon-photon interactions. Decreasing the particle size will affect the energy gap, and therefore, the energy emitted by the photons will possess different frequencies [40–46].

Owing to the fluctuations in the phonon-photon interactions, or plasmon resonance, between the nanoparticles in matrices or with other particles, different colors are observed for the nanoparticles of different sizes and in different environments. This interaction could be exploited to detect certain molecules or indicate their presence in a certain environment as was illustrated for Ag and Au nanoparticles that could elicit different spectroscopic properties if bound to proteins, DNA, biotin, and avidin [47].

8 Application of optical properties of nanoparticles in drug delivery

The surface plasmon resonance has given rise to the interesting light-triggered drug delivery systems. The application of near-infrared light (NIR) is a very promising source of irradiation as the biological tissues are incapable of absorbing light at this frequency. However, by the modification of the size of Au and Ag nanoparticles, these are capable of absorbing radiation over a broad range from the near ultraviolet to the NIR region to best suit the application [48]. If these particles were then targeted and located in a target tissue like tumor, the plasmon resonance could be exploited to locally heat the particles [49] to induce thermolysis of a tumor if part of a thermally enhanced delivery system releases the encapsulated drug [50]. Both the thermal ablation effect of the gold nanoparticles that are irradiated with NIR and thermally triggered release of doxorubicin could be combined [51].

Owing to the mean free path lengths of phonons, which are typically larger than the size of the nanoparticles, the geometric shape of the nanoparticles can also influence the plasmon resonance effect and, therefore, their response to light [42, 52], and the subsequent therapeutic effect or application can be modified according to size and structure [53]. Figure 3 depicts some of the effects of nanoparticle geometry on optical properties and its potential application.

9 Thermodynamic properties of nanoparticles

9.1 Heat transfer

Classic thermodynamics is generally valid when the number of nearest neighbors in a particular system is large. In the nanoscopic systems, <*NN*> is small; therefore, heat transfer deviates from the macroscopic scale. Macroscopic heat conduction is dependent on a heat

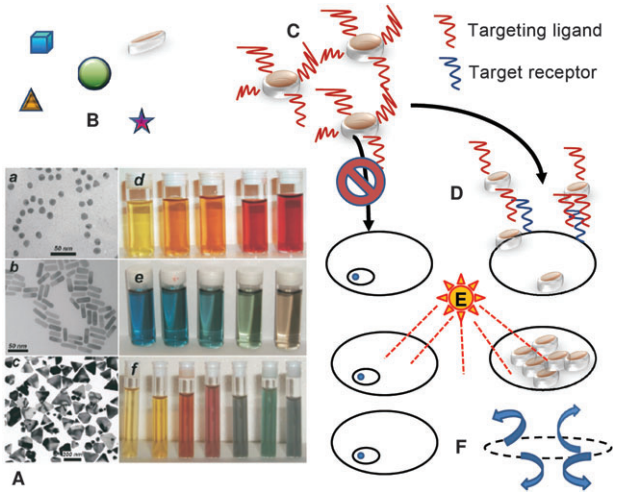

Figure 3 (A) Nanoparticles of different shapes and sizes, (a) Au nanospheres (scale bar is 50 nm), (b) Au nanorods (scale bar is 50 nm), (c) Ag nanoprisms (scale bar is 200 nm), (d) AuAg alloy with increasing fraction of Au, (e) Au nanorods with increasing aspect ratio, and (f) Ag nanoprsims with increasing lateral size [53]. [Reproduced with permission, copyright (2007) by Elsevier.] (B) Selection and loading of drug nanoparticles based on optical and other properties, (C) modification with targeting ligand, (D) delivery of nanoparticle to cells with and without targeted receptor with internalization of nanoparticles, (E) irradiation of cells at selected wavelength to trigger response from the nanoparticles and (F) due to photon-phonon interaction, heat is generated with thermolytic effect and thermally triggered drug release. Normal or nontargeted cells remain unaffected by irradiation.

gradient or a series of adjacent layers with their own local temperature – a situation which is not defined at the nanoscale. Abrupt variations or boundaries in temperature between successive rows of atoms or molecules in a nanosystem cannot be distinguished [11].

A region with a defined local temperature must, therefore, be larger, such as at the macroscopic scale, than the scattering distance of the heat-transferring phonon if the region should remain defined. This definition is compounded by the fact that different phonons vibrate at variable frequencies [54].

The local definition of temperature regions in the bulk is the basis of heat conduction described Fourier's law (Equation 4) [55–57]:

$$q=-k\nabla T \tag{4}$$

where, heat flux is defined by the term q, and the temperature gradient is denoted by ∇T, and finally, the thermal conductivity is noted as the term, k.

Clearly, the Fourier law is invalid for the nanoparticles as the phonon-free path exceeds the distance between the adjacent nanoparticle extremities. Furthermore, the temperature gradient between the nanoparticle extremities is undefined. The heat transport between the nanoparticles is, therefore, defined as ballistic rather than diffusive as found for macroscopic materials. The heat energy is conducted by jumping directly from one nanoparticle to its nearest neighbor, analogous to electron hopping during electrical conduction. Ballistic transfer, therefore, makes the observation of thermal events very difficult at the nanoscale [58–62]. Figure 4 shows the relative size of the phonon wave to particle size and the observation of heat conduction under these conditions.

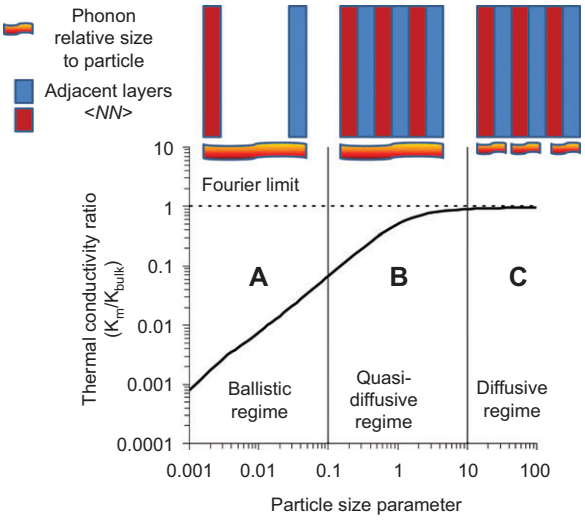

Figure 4 The heat conduction mechanism by phonons in (A) the ballistic regime where particles are significantly smaller than the mean free path of the phonon, <*NN*> is low and a temperature gradient is undefined, (B) the quasi-diffusive regime where particles are small compared to the phonon mean free path, <*NN*> is large enough to define a temperature gradient although localized over several adjacent layers, and (C) the diffusive regime where particles are sufficiently large compared to the phonon so that a temperature gradient is established between nearest neighbors. The particle size parameter is the ratio of particle radius to phonon mean free path [63]. [Reproduced with permission, copyright (1996) by the American Society of Mechanical Engineers.]

9.2 Crystallization

The macroscopic description of crystallization implies that the separation between the solute and solvent will occur at supersaturation in order to minimize the free energy. Phase separation will result in local concentration fluctuations in the mother liquor with the nuclei forming through the aggregation of solute clusters, which can also redissolve. Therefore, a statistical size fluctuation in the crystallite size is seen until the critical radius is attained, and the nuclei become dissolution resistant. The nucleation rate is described by Equation 5 [64]:

$$B=K_1\exp\left(-\frac{\Delta G_{CT}}{kT}\right) \tag{5}$$

where B is the rate of nucleation, K_1 is the system constant, k is the Boltzmann constant, ΔG_{CT} is the critical free energy for nucleation (at supersaturation), and T is the absolute temperature at the point of nucleation [64].

Equation (3) can be rewritten in terms of a particle with a spherical radius of r, to describe the free energy change that is needed to nucleate the solute, i.e., the sum of the free energy required form a surface between the solute and solvent and the free energy to form the bulk (Equation 6) [64]:

$$\Delta G=\Delta G_S+\Delta G_V=4\pi r^2\gamma+4/3\pi r^3\Delta g_v \tag{6}$$

where S and V refers to the surface and bulk volume, respectively. γ is the surface tension and Δg_v is the difference in the free energy between the phases.

If nucleation is observed, the radius of the forming particle had exceeded the critical Lewis radius, r^*. Differentiation of Equation (4) leads to the calculation of r, and its minimum value for nucleation is given in Equation (7) [64]:

$$r^*=-\frac{2\gamma}{\Delta g_v} \tag{7}$$

where the terms are the same as in Equation (6).

The supersaturation ratio is defined as the concentration of the solute in the boundary layer as a fraction of the bulk concentration as seen in Equation (8) [64]:

$$S_r = \frac{c_s}{c_\infty} \tag{8}$$

where S_r represents the supersaturation ratio, C_s gives the concentration in the boundary layer, and C_∞ is the bulk concentration.

Equation (8) can be rewritten in the form of a Kelvin equation to account for a small particle or confinement conditions in Equation (9) [64]:

$$\ln\left(\frac{c_s}{c_\infty}\right) = \frac{2\gamma M}{\rho R T r} \tag{9}$$

where M is the molecular weight of the solute, ρ is the density of the solute (concentration), R is the universal gas constant, T is the absolute temperature, and r is the particle radius.

By the substitution of Equations (7) and (9) into Equation (6), Equation (10) is derived to express the change in free energy as the rate of nucleation at the critical radius [64]:

$$B = K_1 \exp\left(-\frac{16\pi\gamma^3 v^2}{3k^3T^3\left[\ln(S_r)\right]^2}\right) \tag{10}$$

where v is the molar volume of the solute, and the other terms take on the previous meanings.

It is now questioned how nanotechnology can influence the crystallization of drugs. The control over nucleation poses one of the most difficult challenges in crystallization due to the induction of interfaces by experimental or production conditions.

9.2.1 Pharmaceutical perspective on nanocrystallization

Recently, acetaminophen and aspirin were confined on the nanoscopic level to influence their nucleation. By variation in the pore size of the polymeric template gels, the nucleation rates of these drugs were optimized. The pore size of the template gels was easy to manipulate to modify pore size, thus, control the nucleation step. Nanoconfinement could make a significant contribution to rational crystallization process design in the future as the nucleation step can now be controlled [65].

The controlled multipoint-confinement method was also used to nucleate aspirin from nanopatterned surfaces where the templating (meth)acrylate and other vinyl polymeric materials exposed different functional surface groups. Aspirin comprises a benzyl ring that is substituted with adjacent carboxylic acid and ester groups, which could interact with the templating material surface groups. The study illustrated that the highest nucleation rates could be obtained if the polarities of the templating polymer and drug matched and if the polymer was nanoporous with confining geometries of 50–100 nm. Owing to the confinement of the solvent molecules that transport the solute molecules, the solute is localized for a longer time compared to a macroscopic, unconstrained environment. Therefore, supersaturation is induced faster and at lower solute concentrations than normally observed at the macroscopic level [66].

Polymorph selection could be another useful application of nanoconfinement of molecules in a polymeric matrix of varying pore size by which r^* could be regulated. As different polymorphs have different r^*, polymorph selection can prevail as was illustrated for ROY and anthranilic acid. The judicious selection of the template matrix could also ensure its selective removal to liberate the free polymorph. The templating matrix could easily be added to the crystallization solution and result in a templated nucleation process, which is not easily achieved from a pure drug solution [67]. Structures that mimic the crystal packing of mature crystal forms could be exploited to manipulate polymorphism, crystal habit, and size [68], implicating that the control over drug crystallization could already be induced at the nanoscopic level.

The utilization of self-assembled monolayers of aminopropyltrioxysilane octadecyltrichlorosilane (OTS) was also used to provide a nanopatterned surface to capture nanodroplets of the solute glycine and guide its crystallization [69]. The OTS layers were also imprinted on inert templates to selectively nucleate certain polymorphic forms of semiconductors such as pentacene, tetracene, rubrene, and fullerene [70].

Perhaps the utilization of dendrimers could provide an even more elegant nucleation platform as these nanomolecules are even better defined than polymeric nanomatrices. The functional groups of dendrimers have been characterized well [71] and could potentially provide a known number of well-defined nucleation sites.

Various poly(amidoamine) (PAMAM) dendrimers were applied to the selectively nucleate, the most unstable polymorph of $CaCO_3$, vaterite. Vaterite is preferred from a technological perspective as it exhibits higher solubility, higher surface area, and higher dispersability. The

generation or size of the PAMAM dendrimers controlled the particle size and size distribution of the resultant vaterite [72]. We predict that drug crystal polymorphism will soon be templated by nanoconfinement in dendrimer crystallization platforms.

Nanoconfinement clearly results in a departure of nucleation from the classic theory. The control over nucleation will become more commonplace in the future and revolutionize crystallization processes away from the current, random nucleation processes. The templating approach will become more feasible as nanoconfinement becomes better understood and as manufacturing of the nanoconfinement templates become commercially viable.

Contradictory to crystalline phases, the stability of amorphous materials can also be ensured. The indomethacin surface crystallization was confined by a layer-by-layer coating technique. The molecular mobility of the surface molecules are numerous orders higher than in the interior bulk of the crystals. Therefore, the critical particle radius preceding nucleation could not be reached with the resulting higher solubility and relative stability of the glass nanoparticles [73]. Figure 5 illustrates the application of nanoconfinement to control crystallization.

9.3 Glass transition temperature

A multitude of materials can solidify as glasses or amorphous materials rather than crystals, and it has been found that finite size effects exist in the glass transition state that affect the stability of low-dimensional materials [74, 75].

Significant interest has been focused on the glass transition temperature (T_g) for nanomaterials for which both decreases and increases of the values were found compared to bulk material transitions. The T_g provides a very practical guide to the maximum processing temperature of the material for many applications [76]. This development was most probably the offspring of a study by Bares [77] that found that the T_g of styrene-butadiene-styrene triblock copolymers decreased as surface-to-volume ratio increased. Bares expanded the dependence of the T_g on the molecular weight as follows from the original form (Equation 11) [78] to the form (Equation 12) [77]:

$$T_g = T_{g\infty} - K_M/M \tag{11}$$

$$T_g = T_{g\infty} - K_M/M - K_S(S/V) \tag{12}$$

where T_g is the glass transition temperature of the material, $T_{g\infty}$ is a constant glass transition temperature of the material where the molecular weight, M, is infinite (therefore constant). K_M is a constant describing the change in glass transition temperature for a specific material of M molecular weight. K_S is a constant that describes the change in the glass transition temperature as a function of the surface-to-volume ratio of the particles in the nanomaterial.

A number of studies have shown that T_g is depressed for ultrathin polymer films of nanoscale proportions compared to the bulk [76] and that the depression was proportional to the thickness of the films. These depressions could tie in with the decrease in the associated <*NN*> of the films as they become thinner [75]. Consequently, lower cohesive energies were apparent, resulting in the depression of T_g of the film.

Not only the nanofilms of the polymers show a lower T_g compared to the bulk but also the organic liquids that are confined in the nanoscale pores of a certain substrate. The nucleation of the liquid could be markedly affected as r^* must be exceeded for the liquid to nucleate. This nucleation is affected by the surface-to-volume ratio of the crystallites and, subsequently, the interaction between the material, pore wall, and liquid. Confinement can be induced by small pore matrices composed of polymer films and gels, porous glass, silica gels and zeolites [79]. Ultimately, this confinement should retain the liquid in a supercooled state and, thereby, the study or preparation of the glass phase of various substances was suggested [80, 81].

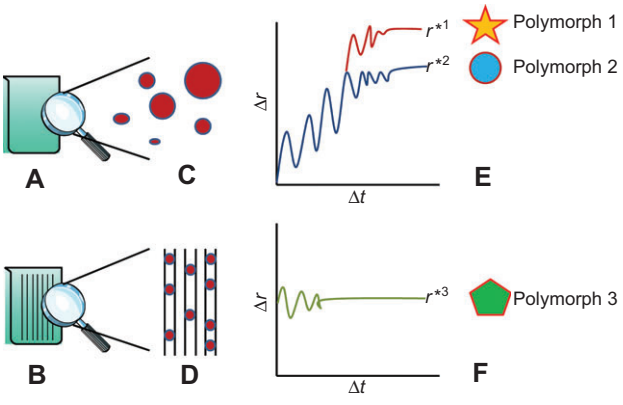

Figure 5 Crystallization starts at the nucleation phase in an (A) uncontrolled, conventional environment and in a (B) nanoconfined, controlled environment. Nucleation is started in an (C) uncontrolled fashion with a wide particle size fluctuation (Ostwald effect) and in a (D) controlled clustering fashion inside templated pores. Owing to ambient conditions and (E) heterogeneous nucleation, several polymorphs form from the solution, whereas (F) nanoconfinement induces controlled supersaturation and multiple homogenous nuclei to produce the selected polymorph.

9.4 Nanoparticle glass transition temperature and drug delivery

Concerning drug delivery, the manipulation of the glass transition of the delivery system can significantly influence its release properties. Generally, for the materials showing lower glass transition temperatures, the mobility of the particles are higher than for the materials with higher glass transitions. Subsequently the release of encapsulated drugs is expected to increase with a decrease in T_g for its carrier as illustrated for poloxamer/poly(lactic acid) (PLA) nanoparticles [82].

Closely related, but in fact the opposite sequence of events to T_g, is the lower critical solution temperature (LCST) of polymeric materials. At this temperature, a polymeric material experiences a sol-gel transition. This phenomenon is dependent on the type of material and also on the particle size. Pluronic® is a triblock copolymer comprising poly(ethylene)-poly(propylene) blocks. At low concentrations of this polymer, micelles form, which show a solution state, useful for rapid drug release. However, at higher concentrations, nanoparticles that are larger than micelles form and in a gel state [83].

This gel is atypical by demonstrating significant hardening and cannot be described as a normal gel state as seen for the other materials exceeding LCST when heated. Owing to this hardening of Pluronic® to form a nanocolloidal glass at slightly larger particle sizes, the dissolution and release of the encapsulated drugs such as procaine hydrochloride could be significantly slowed down. Thus, employing the same type of encapsulation material, but at different concentrations to result in particle size increases, the release characteristics at a set temperature can be markedly influenced [83].

The manipulation of the glass transition temperatures of pharmaceutical materials can greatly enhance the practical exploitation under realistic processing temperatures especially for thermolabile phases. The stabilization of the amorphous phases of drugs by nanoconfinement can also improve the solubility of the drugs and be of use in therapeutics where poor solubility of the drugs prevents their clinical success.

9.5 Melting point

The melting points of nanomaterials also differ from their corresponding macroscopic materials as a consequence of their free surface and size properties. Several examples could be found to illustrate the melting point depression as a function of the particle size, and the reader is referred to these studies [84–87]. The melting temperature is linearly proportional to the reciprocal of the crystal size and can be expressed in Equation (13) [88]:

$$T_m = T_{mb}\left(1-\frac{C}{D}\right) \tag{13}$$

where T_m is the melting temperature of the nanosolid, T_{mb} is the bulk melting temperature corresponding to the material of the nanosolid, D is the crystal size of the nanosolid, and C is a material constant.

Qi [88] further developed Equation (13) as seen in Equation (14):

$$E_{tot} = E_0\left(n-N\right)+\frac{1}{2}E_0N \tag{14}$$

where the number of total atoms of a nanosolid is equated to n and the number of surface atoms as N. The number of the interior atoms in the solid is, therefore, $(n–N)$, and this interior structure could be compared closely to that of the bulk material. The cohesive energy of a single atom in the bulk is set as E_0; therefore, the total contribution of the interior atoms in the nanosolid is $E_0(n\text{-}N)$. Furthermore, half of the total bonds of each surface atom do not contribute to the cohesive energy and, therefore, the contribution of the surface bonds to the cohesive energy is expressed as $E_0/2$, and the total contribution of the surface atoms to cohesive energy, therefore, assumes the form $NE_0/2$.

Equation 14 is further elaborated by the consideration of the Avogadro number, A, to account for the energy per mole of nanosolid, E_p (Equation 15) [88]:

$$E_p = E_b\left(1-\frac{N}{2n}\right) \tag{15}$$

where $E_b=AE_0$. In turn, the cohesive energy and melting temperatures of the material is indicative of the bond strength between the nuclei of the material, and the cohesive energy is linearly proportional to the melting temperature of the material [89]:

As expected, the cohesive energy of the nanosolid is, therefore, a function of the ratio, N/n, and the melting temperature relation can be derived from Equation (16) [88]:

$$T_m = T_{mb}\left(1-\frac{N}{2n}\right) \tag{16}$$

As predicted by W. Thomson in 1871, the ratio N/n is dependent on the particle size [90–95].

The particle shape can affect the n/N ratio in several ways as was apparent for the variation in T_m for the particles of equivalent size, but for geometries of nanospheres,

nanowires, and nanofilms for which n/N varies in the relation 3:2:1 [95]. Therefore, nonspherical particles of the same volume as that of the spherical ones will solidify at a lower temperature. Nanodiscs and nanorods melt at a lower temperature than nanospheres. Under certain conditions, the liquid nanoparticles could act as an adhesive between the solid particles. It is expected that the shape of the nanoparticle would play a significant effect in the nucleation and the reactivity of the particle [94]. The melting point temperature could oscillate under and above the melting point of the bulk material and is attributed to the effect of the particle size on the cohesive energy. Cohesive energy changes are caused by fluctuations in the bond-order length strength for low <*NN*> systems as is determined by geometry, phonon, and surface lattice instability [96].

The studies discussed to this point focused on metallic or inorganic materials; however, organic nanocrystals of benzene, chlorobenzene, and heptane and naphthalene have also shown the identical dependency of the melting temperature on the particle size [97].

An application of the oscillation of the melting temperature could be illustrated by introducing single impurity effects on the melting of the nanoclusters of the materials. By the introduction of a single impurity atom, such as Ni or Cu atom, smaller than the atoms in the nanocluster, inside the cluster, the melting point of a silver cluster could be increased. Though the study was modeled, experimental proof should become apparent in the near future illustrating the selective tuning of the melting temperature and possibly the charge conduction of nanomaterials [98].

9.5.1 Application of melting point depression in nanoparticles in drug delivery

Drugs with poor dissolution properties might show limited *in vivo* absorption. If the drug could be forced to assume a nanoscale periodicity or nanoscale translational order, the dissolution could be significantly enhanced due to the modification of thermodynamic properties, i.e., profound increases in the number of interface boundaries and changes in the melting temperature and enthalpy compared to the bulk. The potential to improve oral bioavailability was observed for nanostructured griseofulvin and nifedipine in cross-linked PVP [99].

It could benefit pharmaceutical science if researchers got familiarized with the developments in the thermodynamics of nanosystems as it will impact research and industry. Additional studies should be consulted for more comprehensive analysis of the thermophysical behavior of the nanosystems compared to the bulk phases [100, 101]. The thermal properties of the nanomaterials are illustrated in Figure 6.

9.6 Solubility and dissolution

9.6.1 Solubility

The macroscopic properties of the solute material and the solute-solvent interfacial properties generally determine solubility. In macroscopic systems, the surface-to-volume ratio is small, and the macroscopic properties dominate the solubility. At the nanoscale, the surface-to-volume ratio is immense; therefore, the solute-solvent interaction cannot be ignored [103].

Several models are used to predict the solubility of the materials based on cohesive energy density [104], melting point, oil-water partitioning coefficient [105], and the molecular surface area [106]. A fractal model [103] has also been utilized to describe small particle dissolution. This model considers that rough nanoparticles are more soluble than predicted by the Ostwald-Freundlich equation. A decrease in the particle size causes a higher surface curvature resulting in a higher free energy and a higher probability of interaction with a solvent, therefore, a higher solubility.

The fractal process is seen as a self-similar process, and therefore, small multiples of an identical geometry is removed from the larger particle to dissolve the particle. The process is, however, not infinite as suggested by the model, but limited over a certain size range and roughness until the particle becomes smooth. The self-similarity of the process is then prevented by surface curvature and tension and the subsequent mismatch to solvent geometry. The size and shape of the solvent molecule influences its interaction with the fractal surface and poses a physical limit to further the self-similar drug removal after a certain critical particle size is reached [107].

With an increase in free energy, the small particles tend to agglomerate and grow, which in turn can decrease the surface area. One has to consider that with a high degree of agglomeration and growth, the surface area available to the dissolution process can be overestimated and that a dynamic change in the magnitude of the surface is seen during dissolution [108].

One of the earliest descriptions of the dependence of solubility on the particle size is given by the Ke1vin equation in Equation (17) [109, 110] that considers vapor pressure for a liquid droplet in equilibrium with its vapor

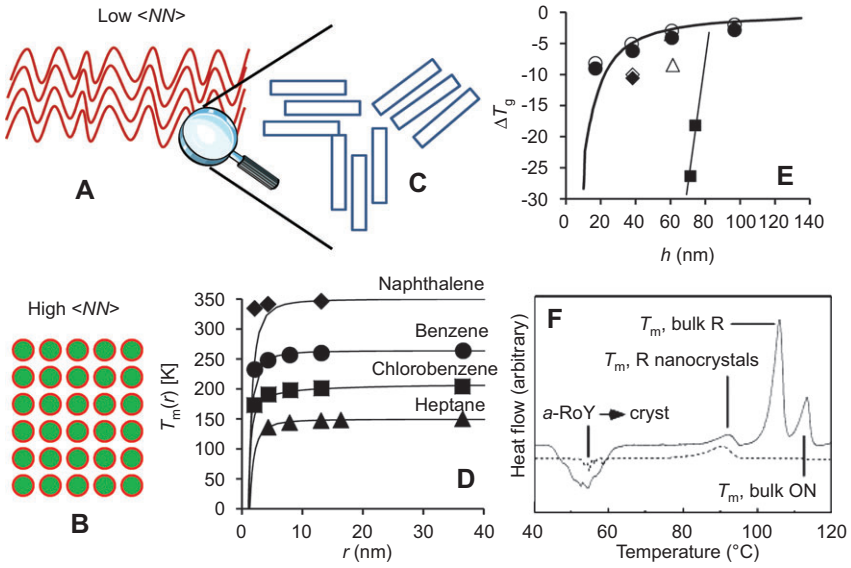

Figure 6 Materials with (A) low coordination <*NN*> such as polymers and amorphous solids have local, but no long-range translational structural order. (B) Crystalline materials show high <*NN*> with local and long-range translational order. (C) Local order in the amorphous material results in small local regions with a local transition from a glassy to rubbery state on heating through the T_g. (D) For crystalline materials, T_m is affected by *r* and decreases with lower *r*. (E) The local order is determined by the local geometry such as seen for different films with different thickness, *h*. The thin line and squares for freely standing PS thin films [102]. [Copyright (2001) by The American Physics Society). (F) The difference in T_m for ROY that was prepared under nanoconfinement and conventional bulk crystallization from its amorphous state. The nanocrystals show a low <*NN*>, subsequently, also a lower T_m relative to the macroscopic crystal [67]. [Reproduced with permission, copyright (2004) by The American Chemical Society.]

pressure and was extended to the Ostwald-Freundlich relationship to consider the solubility terms in Equation (17) [111]:

$$\frac{RT}{V_m}\ln\frac{P}{P_0}=\frac{2\gamma}{r} \tag{17}$$

where R is the universal gas constant, T is the absolute temperature, P is the measured vapor pressure on the vapor side of the liquid-vapor interface for a droplet of radius, r, P_0 is the saturated vapor pressure of the surrounding medium or a flat surface. V_m is the molecular volume of the solute particle, and the surface tension is represented by the term, γ.

Equation (17) can be rewritten in terms of solubility as seen in Equation (18):

$$\frac{RT}{V_m}\ln\frac{S}{S_0}=\frac{2\gamma}{r} \tag{18}$$

where S is the solubility of a small particle, and S_0 is the solubility at equilibrium.

The validity of the Ostwald-Freundlich equation to predict the solubility of small particles is widely debated, although some correlations were found for the spherical particles. The surface tension and <*NN*> for the small particles fluctuate and interfere with the prediction of the Ostwald-Freundlich relation that describes the solubility as a function of the particle size. Corrections have been suggested for both surface charge by W.C.M. Lewis and opposing effects of surface tension (inward pressure on the particle) and electric tension (outward pressure by the particle into the medium) by L.F. Knapp [103].

The limitations of the Kelvin equation is that it describes the macroscopic systems, and as we have seen by now, the macroscopic definitions of density, surface tension, and radius of curvature may not be applicable in nanosystems. Knapp's correction of the Kelvin equation to compensate for the surface charge is given by Equation (19) [103]:

$$\frac{RT}{V_m}\ln\frac{S}{S_0}=\frac{2\gamma}{r}=\frac{q^2}{8\pi Kr^4} \tag{19}$$

where q is the electric charge, and K is the permittivity of the particle dispersion medium with the other parameters as previously described.

The Ostwald-Freundlich-Knapp Equation (Equation 19) implies that an exponential increase in the solubility is not infinite; in fact, a maximum is seen at the Lewis critical radius, r^*. When $r \le r^*$, $S \to S_0$.

The effect of *r* was observed for the solubility of the alloy metal particles that showed a threshold limit for particle

size preceding the exponential increase in solubility. The study did not, however, investigate whether r^* existed for these systems; however, the significant drop in the solubility of the nanoparticles below a certain size alludes to this drop in solubility [112]. In a study of apatite particle dissolution, the r^* was, however, observed with a subsequent decrease in particle solubility below r^* [113]. Similar results were observed regarding r^* of particles and its effect on the dissolution of the nanosupsensions of poorly water-soluble drugs including itraconazole and paclitaxel (PTX) [114].

The solubility of the nanoparticles clearly differs from their corresponding bulk materials, and the effects of surface tension, which is related to particle size, will be a subject of intense research in the near future. The fluctuation in the solubility is also an interesting subject, and solubility should again not be investigated without consideration of the other properties including T_g, T_m, free surface energy at the nanolevel, and nanoconfinement. Figure 7 renders a depiction of the effect of particle size on dissolution.

9.6.2 Dissolution

Dissolution is a kinetic, usually diffusion-controlled process, and the rate of dissolution is defined as the mass of drug dissolved at a given time as expressed by the Noyes-Whitney equation (Equation 20) [115]:

$$\frac{dM}{dt}=\frac{DA}{h}(C_S-C) \tag{20}$$

where dM/dt is the mass rate of dissolution, D is the diffusion coefficient of the drug in solution, A is the surface area of solid in contact with the dissolution medium (assumed constant during dissolution), C_S is the solubility of the drug, C is the concentration of the drug at time t, and h is the thickness of the diffusion boundary layer at the solid surface.

However, during dissolution, the surface-to-volume ratio of the particles changes; therefore, the dissolution rate was normalized for the decrease in surface area, assuming that particle shape was maintained (Equation 21) [116]:

$$M^{1/3}=M_0^{1/3}-kt \tag{21}$$

where M_0 is the mass of the drug particles prior to dissolution, M is the mass of the undissolved drug particles at time t, and k is the cube-root dissolution constant defined as Equation (22):

$$k=\left[N\rho\frac{\pi}{6}\right]^{1/3}\frac{2DC_S}{h\rho}=\frac{M_0^{1/3}}{d}\frac{2DC_S}{h\rho} \tag{22}$$

where N is the number of particles, and ρ is the density of the suspended drug, particle diameter is given by d, and the thickness of the diffusion boundary layer is h. If the drug particles with different d are present, a new correlation model between particle size distribution and dissolution rate was proposed. In this model, the volume-weighted contribution of each particle size fraction to the overall rate of dissolution is calculated [117].

Felodipine particles of various sizes were studied with higher dissolution rates found for smaller particles compared to larger particles. However, a plot of the surface-specific dissolution rate vs. particle size established that an increase in the area alone could not explain the increase in the dissolution rate for small particles [118].

This effect was explained by a decrease in the diffusion boundary layer thickness that scaled with the drug particle radius. The effect of the particle size on the thickness of the diffusion boundary layer was investigated [108]. For particles smaller than 5 µm, the agitation intensity did not significantly change the surface-specific dissolution rate, whereas the dissolution rate was significantly increased at higher agitation intensities for the particles in the range between 15 and 25 µm. It was concluded that

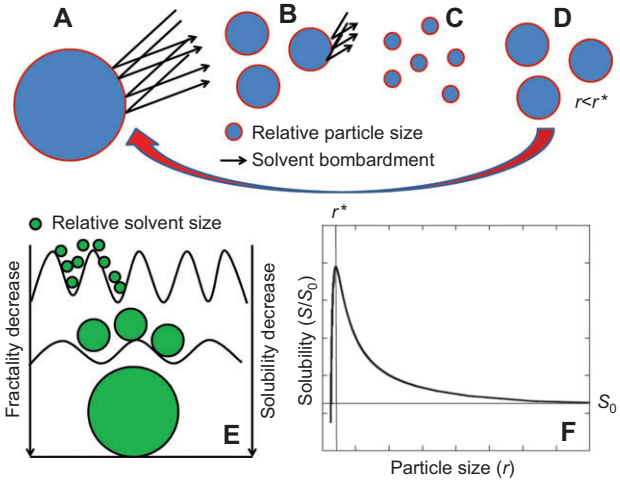

Figure 7 A particle is (A) bombarded by solvent molecules to initiate dissolution followed by (B) size reduction of the particle to form smaller particles that undergo further dissolution until (C) the solute particles are very small with the radius smaller than the critical radius, $r<r^*$, and (D) agglomeration and nucleation is reinitiated with resultant particle growth. The particle surface roughness or fractality (E) decreases over a finite size range as dissolution proceeds to the point where the relative sizes of the solute and solvent molecules are unfavorable for further dissolution and maximum dissolution is achieved. (F) The size-dependent fluctuation in fractional solubility, S/S_0, as the dissolution proceeds to r^* followed by (F) renucleation [103]. [Reproduced with permission, copyright (2007) by Elsevier.]

a reduction in the boundary diffusion layer thickness, in addition to an increased surface area, resulted in the observed increase in the dissolution rate as explained with the Prandtl-Boundary-Layer equation, Equation (23) [108]:

$$h_H = k \cdot L^{1/2} / V^{1/2} \quad (23)$$

where h_H is the hydrodynamic boundary layer thickness, L is the length of the surface in the direction of the flow, k is a constant, and V is the relative velocity of the flowing liquid vs. the flat surface. The higher curvature of the smaller particles results in a reduced surface in the direction of the flow, L, and therefore in a thinner diffusion boundary layer.

An indirect experimental determination of the diffusion boundary layer thickness showed that for particles, 0.53 to 5.9 μm, the effective diffusion boundary layer, h_{EFF}, was directly proportional to the particle diameter for the smaller particles. Moreover, the dissolution rate is indirectly proportional to the square of the particle diameter [119].

However, the smaller particles do not always result in higher surface specific dissolution rates. By using the Heywood shape factor [120], a combined effect of the particle size and shape on dissolution rate was investigated for the small spherical particles (with the shape factor of approximately 6). The small spheres dissolved faster than the large, irregular particles (with shape factors>6) due to a change in the diffusion boundary layer (enhanced degree of irregularity yielded a thicker diffusion boundary layer) [121]. This effect seems contradictory to the fractal model for solubility; however, the particle sizes, wettability, and surface chemistry can affect the dissolution process in unforeseen ways.

Additionally, the surface interaction with a solvent can fluctuate as seen for a decrease in the crystallinity of ZnS in an aqueous environment compared to methanol. The addition of water resulted in strong interactions between the surface of the nanoparticles and water and, hence, in a reduction of the interfacial energy. This structural modification due to the surface environment can also have an influence on the dissolution rate of the nanoparticles [122].

Limited studies focused on the effects of surface tension and wettability on the dissolution of pharmaceutical nanoparticles. The surface tension of the Lennard-Jones films, polymeric and metallic nanosized droplets (2–10 nm radius) was lower than the bulk values; however, it approached the bulk values with $r>r^*$ [123]. In another study, it was found that the wettability of the nanoparticles (>1 nm) can be described by the Young's equation for high surface tension interfaces and presents one example where a macroscopic description found its application at nanoscale [124]. The wettability of the aligned CNTs was successfully manipulated by changes in surface structure and chemical modification, adjusting the surfaces from hydrophilic to hydrophobic and even to superhydrophobic [125].

In summary, the dissolution of a drug from small particles occurs in two steps [126]. First is the interaction between the solute and the solvent resulting in the dissociation of the drug molecules from the solid (solvation step), and the second step is the diffusion of the drug molecule into the bulk dissolution media. Usually, the diffusion is the rate-limiting step [127], and the mathematical models describing the dissolution process are based on the Fickian diffusion laws. The dissolution rate, described as a diffusional process, is directly proportional to the surface area and drug solubility and is indirectly proportional to the diffusion boundary layer. For small particles, the surface area as well as the solubility is increased, and the diffusion boundary layer is decreased. Therefore, the challenges arise to determine if the dissolution is diffusion controlled for the nanoparticles and if the diffusion boundary layer still existed. Figure 8 illustrates the dissolution process.

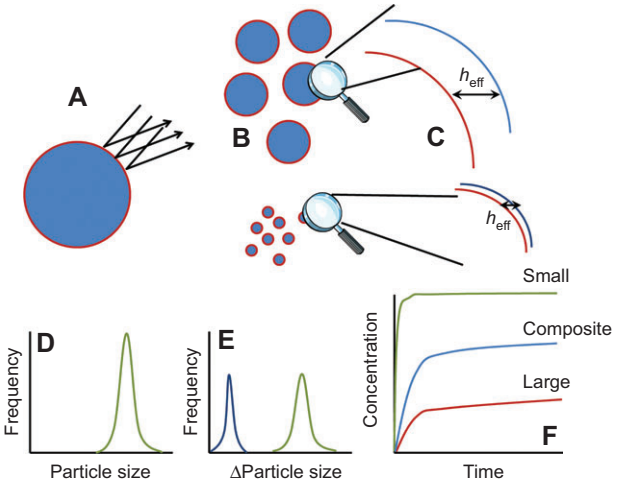

Figure 8 (A) A solute particle dissolves due to its interaction with solvent molecules in the dissolution environment. (B) Owing to the dissolution, the particles are produced with (E) a multimodal, dynamically shifting size distribution that is not equal to (D) their initial size distribution. In addition to the fluctuations in the size distributions that determine the surface area for dissolution, (C) larger and smaller particles show differences in <*NN*> so that smaller particles have a significantly thinner diffusion boundary layer, h_{eff}, compared to larger particles. (F) Two extremes represent the dissolution profiles of small and large particles; however, a composite curve is more likely describing the overall process due to a dynamic shift in particle size distribution during dissolution.

10 Nanopores

We have seen in the previous sections that the surface-to-volume ratio changes as the particles become smaller. If the nanopores are induced into a macroscopic material, the same effect is observed. However, by tailoring the pores, nanoconfinement effects can be imposed on a material, and as we saw, the electrical and thermal conductivity properties as well as optical responses can be affected by nanoscale geometry and, thus, confinement.

Figure 9 shows that pore-filling takes place in two steps, i.e., adsorption followed by condensation. Figure 9A also shows the Kelvin equation and, Figure 9C, the modified Kelvin equation that describes the effect of curvature on the approaching or filling phase on the pore [130]. The adsorption and condensation steps are competing processes and that the contribution of the adsorption affects the condensation step. The adsorption contribution was described by the Brunauer-Emmett-Teller (BET) equation (Equation 24) [130] that substitutes the surface coverage of the pore walls by the adsorbed water in terms of pressure and the adsorption isotherm:

$$\frac{n}{n_m}=\frac{C_x}{\left(1-x\right)\left(1-x+C_x\right)} \tag{24}$$

where x is the ratio P/P_0, n is the amount of adsorbed liquid at the pressure p, n_m is the amount of fluid sorbed for a monolayer of the liquid, and C is the term describing the energy of adsorption.

The prevalence of condensation is even higher as the pore size decreases [131] and deviates significantly from a simple prediction made by the Kelvin equation (Figure 9). The adsorption of liquids to the surface walls of the pores in the nanoscale range is very probable as seen from their high surface area and subsequently high-surface free energy.

Hydrogen gas, as a potential alternative fuel, illustrated a significantly higher storage in nanoporous vinyl

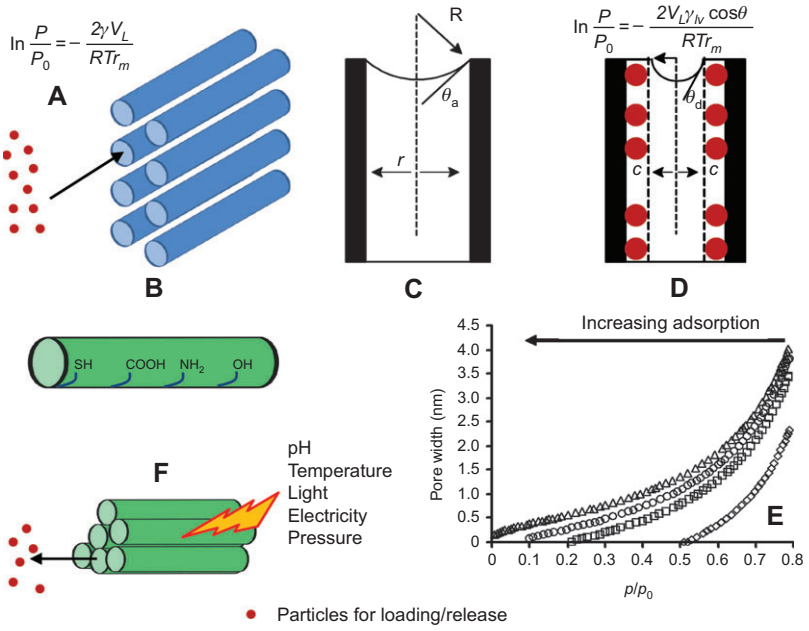

Figure 9 (A) The diffusion of small particles into nanotubes are determined by several factors as described by the Kelvin equation [127] (copyright (1998) by the American Chemical Society). The pressure, P, experienced in the tube relative to the vapor pressure, P_0, of the bulk phase, interfacial tension, γ, molecular volume of the adsorbent, V_L, radius of the interface curvature, r_m, as well as (B) the surface chemistry of the nanotube wall, relative polarity of the solute and solvent molecules, and surface roughness. The filling of pores takes place in two steps [127, 128]. [Reproduced with permission, copyright (1997) by the American Chemical Society.] (C) The initial adsorption of the solute onto the inner pore wall in monomolecular or multiple layers. This adsorption step is dependent on the solute-pore wall interaction and the contact angle of this interface, θ_a, as determined by the pore wall distance, r, and the curvature radius, R, between the interface of the solute and pore wall. The second step in filling (D) must be preceded by adsorption, and the Kelvin equation is modified to compensate for the adsorption step. The adsorbed layer results in a reduction of pore wall distance. The curvature of the solvent-adsorbed layer results in a more favorable contact angle, θ_c, for condensation. The effect of the extent of adsorption on the vapor pressure for tubes of various pore diameters is seen in (E). Lower pressures are needed for the condensation at higher extents of adsorption as seen for N_2 at 77.4K [129]. [Reproduced with permission, copyright (2002) by the American Chemical Society.] (F) Loaded nanotubes can expel their content based on various stimuli. The inner (condensed) phase releases with greater ease than the adsorbed phase.

polymers compared to the microporous equivalents [132]. Therefore, the contribution of capillary adsorption to moisture sorption becomes very significant in nanocapillaries [133], especially where interactions between the liquid-solid interface are stronger than the liquid-liquid interface interactions [134]. The effects of P/P_0, temperature, and pore geometry were also investigated for argon, krypton, and nitrogen that were confined in porous silica materials. The evaporation of the gases was controlled by the temperature, pore geometry, and the relative pressure of the systems [135].

If water molecules were confined between weakly attractive hydrophobic pore walls, the contact angles would exceed 90°. If the wall to wall distance was small, spontaneous evaporation of the water would be possible [136]. A threshold for the interwall distance for the evaporation of water confined between two hydrocarbon walls is predicted on the order of 100 nm and is characterized by a contact angle of 110° [137–139].

In the opposite case where a liquid, i.e., cyclohexane is able to wet the pore surface of a mica capillary, the contact angle can assume <90°, and the liquid would condense under confinement. Evaporation will take place if the pore widens again, and the relative pressure is alleviated [140].

10.1 Applications of nanoporous materials in sorption and drug delivery

Water is one the most important transport media in chemical and biological systems, for example, with ion channels through membranes [141]. The water molecules also behave differently under nanoconfinement and also differently compared to some organic molecules, which, as was discussed earlier, tend to show solidification under confinement due to solute transport restriction. Water shows a small increase in viscosity under nanoconfinement and allows the entry of water into the nanopores even in hydrophobic channels. This would seem unlikely due to the intermolecular hydrogen bonding between the water molecules at the macroscopic level; however, a large proportion of these molecules are not bound efficiently to each other due to the fluctuations in the coordination of the water molecules. However, in the nanopores, the intermolecular hydrogen bonding between the water molecules is significantly preferred to the interaction with the pore wall, and the water moves in a "single file" through the pore walls [142].

The effect of the nanopore size on water and drug permeation is one aspect that requires investigation. Pores below 1 nm are found in CNTs, zeolites, and ion channel proteins potentially useful for nanoparticle drug delivery. Beckstein et al. [143] simulated the movement of ion permeation through the nanopores. They found that the ions were still excluded from the pores even though the pore radii exceeded the ionic radius. The resistance of the ion permeation through the pores was attributed to the hydration shell of the ions that increased the effective size of the permeant.

The transport of the water molecules through the nanopores is also seen as intermittent, i.e., the pore mouth has to be filled with water, followed by entry into the channel and then chain transport. This process is sensitive to the pore radius, and as the pore wall radius fluctuates due to the fluctuations in the pore wall attraction distances, the liquid can either enter or be excluded dependent on the critical pore radius [144] and the fluctuation in the filled and empty state of the nanochannel [145].

Several solid materials such as zeolites, minerals, biological hydrogels, and surfactant assemblies present cracks and pores in their structure that are permeable by gases [146]. Adsorption of, for example, water vapor into these pores could, therefore, be possible. It is known that the adsorption of a liquid layer on a capillary wall could result in the transition of a vapor to a liquid [147].

Additionally, the changes in the pH of the medium could also influence the degree of ionization of the pore walls and, therefore, the interaction between the permeant, transport liquid, and pore walls. The selective anion or cation transport could subsequently be envisioned as a function of the transport liquid pH [148]. This effect of polarization in CNTs was also found to be species-dependent, as Cl^- hydration was more dependent on the confinement effects than on Na^+, as chloride also preferred to orientate in the center of the pore and, sodium, closer to the inner surface. The ionic size of the chloride is also larger than sodium resulting in the differences in their sorption [149].

Ibuprofen and Rhodamine 6G was loaded into nanoporous silica matrices of which the pore walls were functionalized with different silanes that had substituents of various polarity. The pore walls, thus, exhibited a difference in its hydrophilicity and could capture the drugs, to a greater or lesser extent, as well as determine the release rates of these drugs [150]. Similarly, the interaction between the functionalized mesoporous silica and cisplatin could be optimized by the guest-host interaction. The surface area and density of the functional groups significantly affected the release of the drug from these pores and also the variation in the temperature influenced the interaction by the alteration of the hydrogen bonding capacity in the pores [151].

Ibuprofen was loaded and confined into a mesoporous silica matrix by exploiting the capillary wetting of ethanol as the solvent. The ibuprofen was solidified in an amorphous form and was studied with several techniques. It was found that ibuprofen was arranged in two zones of the nanocapillaries, namely, those closer to the inner wall and those in the center of the lumina. It was found that the ibuprofen that assumed a *cis* conformation possessed a lower dielectric constant and, therefore, adsorbed to the inner wall. By increasing the temperature, the ibuprofen molecules underwent a *cis-trans* conversion, and the *trans*-form was repelled from the inner wall and, subsequently, showed a higher mobility in the interior. The drug release kinetics could, in the future, be modified according to the guest-host interaction and the adjustment of the ambient conditions such as temperature [152].

Inorganic zirconium discs can be loaded on the alumina substrates with a pore size of 3 nm, a diameter of 50 nm, and a thickness of 1 mm. These pores were then functionalized with octyltriethoxysilane. Owing to the hydrophobic functionalization of the pores, water contact angles and the surface tension became unfavorable to penetration compared to the pristine pores. The tracer molecule, azobenzene, showed different diffusivities depending on the degree of the hydrophobicity and the polarity of the medium that was used to study its release [153].

The confinement of the drug molecules in the nanopores to control their release is a different approach from the conventional coating of drugs. Normally, the coats provide a barrier to release by increasing the diffusion path lengths; however, by capturing a drug in a nanopore, the exposure to the release medium can be modified. The layer-by-layer coating method was utilized to coat a glass surface. The nanocoated films were subsequently submerged in media of different pH to induce a nano- or microporous texture, and ketoprofen and cytochalasin D was loaded in the pores. The multilayered structures could also be formed to contain porous and nonporous layers, which showed different refractive indexes as the pores were loaded [154].

The macroporous silica membranes were loaded with doxorubicin and then anodized with Pt/Ir for various times. This anodization produced nanoporous coatings of 200 nm thicknesses capping the microporous drug wells, which showed pore openings of ~2 μm diameter and pore depths of 2 to 40 μm depending on membrane etching time duration. The release of doxorubicin corresponded to the pore properties and coating thickness [155].

Another example of the hybrid nanoparticles was illustrated for the mesoporous silica nanoparticles, which were capped with acid-decomposable zinc oxide quantum dots. The silica nanoparticles were loaded with doxorubicin by the functionalization of the inner pore wall with amino groups, and the nanolids could prevent its release until these particles were internalized into HeLa cells. In the cells, the nanoparticles were sequestered by lysosomes in which a slightly acidic environment prevailed, and this dissolved the ZnO nanolids, subsequently releasing doxorubicin. Additionally, the dissolution of ZnO released Zn^{2+} ions that were capable of disrupting the anionic cell membranes for an additional antineoplastic effect [156].

The construction of the so-called bioactive glasses comprising of silica nanoporous scaffolds, which were manufactured on the triblock copolymer Pluronic® 123, possesses hierarchical structural properties that can be modified. At the macroscopic scale, long fibers are formed, and these can be assembled in the membranes with an interconnected macroporous structure. Microscopically, these membranes show very high surface areas due to the presence of nanoscale structures. By selectively dissolving the polymeric surfactant, the silica nanostructure remains, and this structure shrinks due to the disappearance of the polymeric support, which lowers the structural entropy of the system. Depending on the degree of the removal of the surfactant, pores ranging from 3 to 450 nm can be produced. By loading of gentamicin in these porous bioactive glasses, the loading of the drug could be adjusted according to pore size. Small pores and midsize pores of 3 to 5 and 3 to 16 nm, respectively, showed the highest gentamicin loads of 12.7% and 14.4%, respectively. The large pores of 32 to 65 nm showed only 5.5% loading due to its lower relative surface area compared to the smaller pores. The change in pore size could also be monitored during loading due to the changes in the surface area measurements by N_2 adsorption isotherms, and the release was also seen to be pore-size dependent. The large pores showed a significantly faster release rate than the smaller pores [157].

Carbamazepine is another drug that has illustrated the benefits of nanoconfinement in the silica nanopores. MCM-141 is a popular silica matrix with mesoporous properties where pores assume the size range of 2–10 nm. MCM-41 exhibits a very high surface area with uniform pore size, which is seen through the complete cylindrical length of the pore to provide tortuosity and narrowing effects on release and very efficient confinement properties upon solvent evaporation to prevent recrystallization. The confinement is the result of the guest-host interaction between the silanol groups of the silica and amide groups in carbamazepine. However, this interaction is easily alleviated under physiological conditions where water competitively abolishes the bonding interaction. This

confinement effect could potentially breathe life into the use of the unstable amorphous form of carbamezipine, which has not found commercial application yet, as the amorphous form can be stabilized in MCM-41 compared to the pristine glass [158].

Acetamimophen is another example where the glassy state could be stabilized in nanoconfinement. Vycor® shows a very uniform nanoporosity with a high degree of silanol groups exposed in the pore inner wall that can undergo hydrogen bonding with the acetaminophen molecules. The pore diameter of the glass was uniform at approximately 4 nm, which is below the critical radius, r^*, of ~4.6 nm for acetaminophen as was calculated by the Gibbs-Thomson equation (Equation 25) [159]:

$$d^* = \frac{4\sigma_{cl}T_m^\infty}{\left(T_m^\infty - T\right)\Delta H_m \rho_c} \tag{25}$$

where the critical pore diameter is d^*, σ_{cl} is the surface energy between the crystal and the melt, H_m is the heat of melting, T_m^∞ is the bulk melting temperature, and ρ_c is the crystal density.

Owing to the confinement of the acetaminophen in the nanopores of the glass where $r^* < d^*$, nucleation could not take place. The hydrogen bonding interaction also was sufficiently strong between the pore wall and the drug molecules to slow their movement to undetectable time scales, further stabilizing the glass. Owing to the small clusters of acetaminophen, no inhomogeneities in the surface and vibrations between the paracetamol molecules could be induced, and the glassy liquid free energy was thus in equilibrium, precluding nucleation. Additionally, the clusters that did form are very uniform due to the uniform pore size distribution [159].

Sirolimus was loaded into a nanoporous array that was formed by spin coating of a block copolymer that consisted of poly(styrene) and PLLA. The coated film was immersed in sodium hydroxide solution that selectively dissolved the lactide blocks. By varying the lengths of the blocks in the copolymer, lamellar or cylindrical pores were produced with pore diameters between 20 and 60 nm. The smaller pores resulted in a controlled release effect that was sustained over several days, whereas the larger pores showed a cutoff size above which the confinement effect was not strong enough to curb burst release. In general, the lamellar pores also stunted the release to a slightly larger extent than the lamellar pores [160].

A number of titanium oxide nanopowders were selected as nanoporous carriers for ibuprofen. The different powders showed pore sizes ranging from 2.5 to 70 nm, and these pores could show mono- or bimodal size distributions. As has become apparent, the too small pores did not allow high extents of loading or release and the too large pores could not control the release. The monomodal pore size distribution also resulted in a significantly better control over loading and release [161].

A few examples could be found where conductive nanoporous materials were used for drug release. PPy is one such conductive polymer in which p electrons are conjugated and can be charged and discharged on electrical stimulation. The stimulus creates a reaction in which the polymer switches between the oxidized and reduced state resulting in conformational changes that displaces and loads the hydrated ions into and from the bulk. PPy was polymerized onto poly(styrene) nanobeads and loaded with fluorescein. The poly(styrene) beads were selectively dissolved, resulting in a nanoporous PPy structure with the dye on the pore outer walls. Upon the electrical stimulus, the electrostatically bound fluorescein was released on PPy reduction and squeezed out of the interstitial space owing to the lack of confinement [39].

It has been proposed that the manipulation of the boiling point of the solvents that are confined in the nanopores could be exploited as a drug delivery system. Below the 2-nm pore radius, the boiling point of water is significantly lower compared to the bulk. At the appropriate temperature, water in the confined space will, therefore, undergo phase transition to form gas, and this will expel the content from the tube lumina. The combination of the different solvents such as water and carbon dioxide under nanoconfinement could provide interesting pressure-activated devices. Heat, light, or electrical conduction could serve to induce the phase transition as the driving force for drug expulsion [162].

10.2 Drug loading

10.2.1 Mechanisms of drug loading

Drug loading can be performed during nanoparticle formation or after the preparation of the nanoparticles [163]. Extensive drug adsorption to the surface of the preformed nanoparticles is possible due to the immense surface-to-volume ratio, resulting in a high initial burst release [164–166]. Furthermore, postproduction loading generally results in a lower drug loading [167–170], and THE loading incubation time also invariably affects the drug loading [169]. Additionally, the strength of the intermolecular force interaction between the drug and carrier system [164] will determine the particle loading efficiency [171]; however, it will hamper the release rate [172–176]. Sometimes, the

interaction between the drug and matrix has to be neutralized by, e.g., introducing ions (buffer solutions) to enable the release from the carrier, i.e., a dendrimer-methotrexate inclusion complex released methotrexate in PBS buffer, but not in water [177, 178].

Drug loading was enhanced by increasing the nominal drug quantity [178, 179]. However, if the maximum loading capacity of the nanocarrier is reached, further increase in the nominal drug loading can even decrease the efficiency [165, 180].

Considering how the physicochemical properties changes as the carrier size changes to the nanoscale, it should be realized that drug loading will not adhere to the known macroscopic formulation principles. Therefore, judicious delivery system design and optimization should be based on the physicochemical properties that were reviewed here.

10.3 Release

10.3.1 Drug release from homogeneous and granular matrices

Uniformly dispersed drug molecules in a nondegradable polymer matrix system (nanospheres) or for which the polymer degradation occurs after the drug release, have to dissolve and diffuse through the matrix to be released. The Higuchi equation (Equation 26) [181] describes the diffusion-controlled release transport rate that is proportional to the square root of time:

$$Q=[D(2C_T-C_S)C_St]^{1/2} \tag{26}$$

where Q is the amount of drug released at time t and per unit area of the exposed matrix surface, D is the diffusion coefficient of the drug in the polymer matrix, C_T is the total concentration, and C_S is the solubility of the drug in the polymer matrix. In the case of a porous matrix, the Higuchi equation is extended by the porosity (e) of the matrix and the tortuosity (t) of the capillary system and is expressed as Equation (27):

$$Q=\left[\frac{D\varepsilon}{\tau}(2C_T-\varepsilon C_S)C_St\right]^{1/2} \tag{27}$$

Despite the porosity, Equations (26) and (27) indicate that the release rate is directly proportional to the surface area, the total amount of drug incorporated in the matrix (drug loading), the solubility of the drug in the polymer matrix, and the diffusion coefficient of the drug in the polymer matrix. The interaction between the drug and polymer is expressed by an alteration of the diffusion coefficient, which is inversely proportional to the strength of the interaction [164]. The Higuchi model fitted the release of beclomethasone dipropionate and indomethacin, respectively, from polymeric micelles [180, 182].

The release rate from the spherical particles with a radius of smaller than 1 mm were studied and pointed out that the interfacial transfer kinetics becomes rate-limiting (analogous to the dissolution arguments) [183]. Short time periods are described by Equation (28) and long time periods by Equation (29):

$$M_t=Ac_0rk\tau \tag{28}$$

$$M_t=\frac{1}{3}Ac_0r\left(1-e^{-3k\tau}\right) \tag{29}$$

where M_t is the released amount of drug at time t, A is the surface area, t is a normalized parameter, c_0 is the initial drug concentration in the particle, r is the radial distance from the center of the sphere, and k describes the interfacial transfer process.

A simple, empirical equation describes that the first 60% of the release was derived where the diffusional exponent n characterizes the release mechanism Equation (30) [184]:

$$\frac{M_t}{M_\infty}=kt^n \tag{30}$$

where M_t/M_∞ is the fractional solute release, t is the release time, and k is the constant describing the characteristics of the polymer matrix and the drug. Release transport can be classified according to the diffusional exponent that has different values for the various swellable as well as nonswellable carrier systems [184, 185]. This empirical equation was, for example, employed to identify the mechanism of the release of bovine serum albumin from nanospheres [186].

Matrix erosion can also result in drug release. The degradation kinetic of the polymers is complex, and reference to the literature is advised [187, 188]. Briefly, the particle size might affect the degradation rate as found that the degradation rate of PLGA during the initial phase was higher for 100 nm particles than for 1 or 10 μm particles. Additionally, the hydrolytic degradation rate of nanofibrous poly(L-lactic acid) foams was accelerated by the larger surface area compared to the solid-walled foams [189]. This case is discussed in further detail in the following section.

Some attempts to model the release pattern from nanoparticles have been performed. Jo et al. [190] and

Polakovic et al. [191] used diffusion or dissolution models. The diffusion model could be used to describe the release from nanoparticles with a low drug loading where the drug was molecularly dispersed. For crystallized drug forms at higher loads, the release rate was, however, dissolution-controlled [191]. The influence of hot and cold homogenization techniques on the release profile of prednisolone was illustrated [192]. The burst release was more significant for the solid lipid nanoparticles prepared by hot homogenization, with highly drug-enriched outer layers.

The double emulsification of bovine serum albumin (BSA) into nano- and microspheres showed an elevated burst release compared to the particles prepared by a novel method employing thermosensitive Pluronic®F-127 gel. It was revealed that double emulsification yielded a higher surface adsorption of BSA compared to the novel entrapment method [186].

10.4 Drug release through polymer shells

If a drug is encapsulated into nanocapsules, the drug has to traverse the capsule shell prior to reaching the medium. The mass rate of permeation, dM/dt, of a drug through the capsule shell can be written according to the first law of Fick under sink conditions, Equation (31):

$$\frac{dM}{dt}=\frac{DKAC_D}{h} \tag{31}$$

where D is the diffusion coefficient of the drug in the capsule shell, A is the surface area, K is the partitioning coefficient of the drug between the capsule interior and the shell, C_D is the solubility (solid) or concentration (dissolved) of the drug in the interior of the capsule, and h is the thickness of the capsule shell. To compare the various systems with different capsule shells with each other, the permeability coefficient is used as it is independent of the surface area and the concentration of the drug on the donor side C_D. The permeability coefficient, also known as the permeability, P, of a polymer shell is described by Equation (32):

$$P=\frac{DK}{h} \tag{32}$$

In practice, the two transport mechanisms, i.e., pore diffusion and permeation through the capsule shell, cannot always be distinguished. Therefore, the decrease in permeability is sometimes explained by the formation of pores in the polymer shell where the drug diffuses through the pores rather than permeates through the polymer shell [193].

Particular interest has been focused on the polyelectrolyte capsules as a drug delivery system. Loading of and release from polyelectrolyte capsules is not part of this discussion, and the readers are referred to the literature [194, 195].

11 Comparison of nanosized with microsized drug carriers

Only a few studies have been performed to compare the release from microparticles and nanoparticles, although not all of the parameters were regulated, except for the particle size. The immense surface-to-volume ratio of the nanoparticle results in the high surface adsorption of drug molecules [196] and also a decrease in the diffusion distance from the core. Gref et al. [197] prepared cyclosporine A (CyA)-loaded PLA-poly(ethylene glycol) (PEG) micro- and nanoparticles and compared them to conventional PLA particles. The nanoparticles revealed a higher amount of surface-adsorbed CyA compared to the microparticles that, therefore, resulted in a high initial burst release. Interestingly, the two different microparticulate carriers (PLA-PEG vs. PLA) exhibited different release rates, but not the nanoparticulate carriers.

5-Fluoruracil was entrapped into the matrices of poly(3-hydroxybutyrate-*co*-3-hydroxyhexanoate) (PHBHHx) micro- and nanoparticles via an emulsification process assisted by sonication. Sonication removed some drug from the nanoparticle surface and forced the adsorption of the drug into the core, whereas the microparticles showed a significant amount of drug trapped in the particle close to the surface. Subsequently, the burst release was obscured for the nanoparticles with a longer release period than what was seen for the microparticles [198].

The efficacy of the nanoparticles could, however, be superseded by the microparticles, and the nanoparticles could fail compared to the microparticles. PTX was loaded into the PLGA particles that attained sizes of 315 nm, 1 μm, and 10 μm with high loading efficiencies of 95%. A significant burst release was observed for the nanoparticles in the first 6 h, which released 50% of its content. The microparticles showed only 30% release in the first 6 h and sustained release after that for 14 days. The microparticles also resulted in tumor growth arrest in the animal model, whereas the nanoparticles were internalized by cells and cleared from the body. The microparticles showed strong cellular association without uptake into the cells and were, therefore, more effective [199].

The PLGA particles of 100 nm, 1 μm, and 10 μm were prepared utilizing poly(vinyl alcohol) (PVA) as the surfactant to encapsulate the model protein, BSA. In the release medium, all the particles showed biphasic degradation patterns with an initial higher degradation rate during the first 20–30 days. The nanoparticles showed a higher initial rate of degradation and, the microparticles, a slower degradation; however, the 1-μm particles surprisingly degraded slower than the 10 μm particles [189].

The second phase showed a similar degradation rate for all the particles. The effect of PVA was identified as the cause of the degradation profiles. The nanoparticles showed a higher surface-to-volume ratio and a larger exposure to the media for degradation; however, PVA could also form a barrier to the diffusion of the media in the second phase. The particles degraded in the first phase with pore formation and fusion of the particles took place. Thus, the pore texture, aggregation, and size parameters became similar by the time the second phase was reached, and the second degradation phase showed uniform characteristics for all the particles [189].

The cumulative release of BSA was highest from the 1-μm particles (~32%), followed by the 100-nm particles (~20%), and these completely outperformed the 10-μm particles (~7%) over 90 days. It was found that the 1-μm particles released the highest fraction of unaggregated protein. This result pointed to the optimization of the formulation conditions to ensure the balance between the particle size and the formulation variables to ensure optimal performance [189].

Another study that illustrated that the optimization of size and formulation will determine the success of the dosage form was illustrated for gentamicin that was loaded in the PLGA micro- and nanoparticles. The PLGA polymers had different molecular weights with free substituted carboxyl endgroups. The microspheres encapsulated more drug than the nanoparticles for the same type of polymer with a higher efficiency for more hydrophilic, unsubsituted polymers due to hydrogen bonding. However, the higher hydrophilicity also resulted in a higher absorption of the release medium into the particle with subsequent higher initial burst release. Depending on the combination of these factors, efficient micro- and nanoparticles could be formulated, and in this case, the nanoparticles from the free endgroup PLGA with a 50:50 composition and 13.7 kDa weight outperformed all other formulations with only 21% burst release in the first hour followed by a sustained release over a period of 1 month [165].

The proangioenic compound SHA-2-22 could prove valuable in improving vascularization in the tissue engineering, and this compound was incorporated in the PLGA nano- and microparticles of approximately 200 nm and 20 μm, respectively. The release of the drug showed a significant burst release of ~85% from the nanoparticles within the first hour followed by a sustained release for another 15 days. The initial burst was between 5% to 20% for the microparticles with sustained release reaching almost 100% over the following 15 days. The drug was captured closer to or on the surface for the nanoparticles, whereas the drug was entrapped deeper into the matrices for the microparticles. It was suggested from this study that a combination of nano- and microparticles could be formulated to attain a high initial loading dose that could be sustained by the microparticles to achieve a constant drug concentration [200].

Prednisone was captured in micro- and nanoparticles of poly-α,β-[*N*-(2-hydroxyethyl)-L-aspartamide]-*g*-poly(ε-caprolactone). Not surprisingly, the release of the drug showed higher release rates from the nanoparticles than from the microparticles; however, the hydrophilicity and degradation of the polymer could be modified to retain the drug in an adjustable fashion and, therefore, lengthen its duration of release [201].

All the examples discussed here showed the common problem of burst release that is often associated with the nanoparticles. We have seen that the solubility and dissolution of the various drugs can increase due to size reduction; however, it seems challenging to harness the usefulness of these properties. The encapsulation of the nanoparticles in the microparticles has, however, illustrated a significant reduction in the burst release as well as enabled the prolonged release of the drug. Ibuprofen and triptorelin acetate were captured in the nanoparticles comprising of poly(ε-caprolactone), and these were subsequently encapsulated in the microparticles, fabricated from Eudragit® copolymers. A double barrier to diffusion was, therefore, induced, first, through the nanoparticle wall and, then, through the microparticle wall. The poorly water-soluble ibuprofen showed a 71% burst release from the pristine nanoparticles due to its higher solubility in size reduction, whereas the burst could be dampened to approximately 20% based on microparticle encapsulation. Triptorelin, in contrast, is highly water soluble and showed the most significant drop in burst from 60% to below 10% attributed to microencapsulation [202].

An undisclosed, BCS class II model compound was formulated in the micro- and nanosuspension formulations. These suspensions were administered to rates in equivalent doses of the drug, and the pharmacokinetic parameters were determined. The nanosuspensions resulted in significantly higher plasma concentrations for all doses, and this was attributed to a higher solubility of

the drug in the nanosupension formulations compared to the microsuspensions. Furhermore, it was suggested that the elimination mechanisms was saturated at higher plasma concentrations of the drug, further showing the advantage of the nanosuspension over microsuspensions [203].

PTX was formulated as Cremophor® micelles (~13 nm), Cremophor®-free PTX-loaded gelatin nanoparticles (~600 nm), and PLGA (50:50) microparticles (~4 µm). The particles were injected intraperitoneally (IP) to evaluate the IP-plasma transport of the drug and its carrier. The microparticles showed much slower clearance of the drug from the IP cavity, providing the advantage of IP cavity targeting. A significantly lower systemic clearance of the drug was seen for the microparticles despite the lower release of PTX from the microparticles, the lower drug clearance resulted in doubling of the survival times of th IP-bearing test animals. The lymphatic drainage and fast release from the nanocarriers were the probable cause of the lower efficiency of these systems [204].

A limited number of studies have been reported that compared the pharmacokinetic performance of nanodelivery systems to micro- and macroparticulate systems. It would seem that for many cases, the administration of pristine nanoparticles would not be appropriate to ensure a sustained or controlled release of the drug. Generally, the unmodified nanoparticles are cleared relatively quickly from the systemic circulation through the immune cells, lymphatic drainage, or release their drug content quickly to result in a fast systemic elimination. The manipulation of the interaction of the nanoparticles with cells will likely be a future direction to optimize the efficacy of nanodelivery systems.

To fully harness the technological advantages of drug nanoparticles, such as higher solubility and loading capacity, a modification of the particle, such as coating or encapsulation, should be undertaken. The key to fully optimize and realize the potential of the nanocarriers would perhaps be an integration of differently sized components, for example, the encapsulation of the nanoparticles in the microcapsules or nanoporous supports. Figure 10 compares drug delivery from nano- and microparticles.

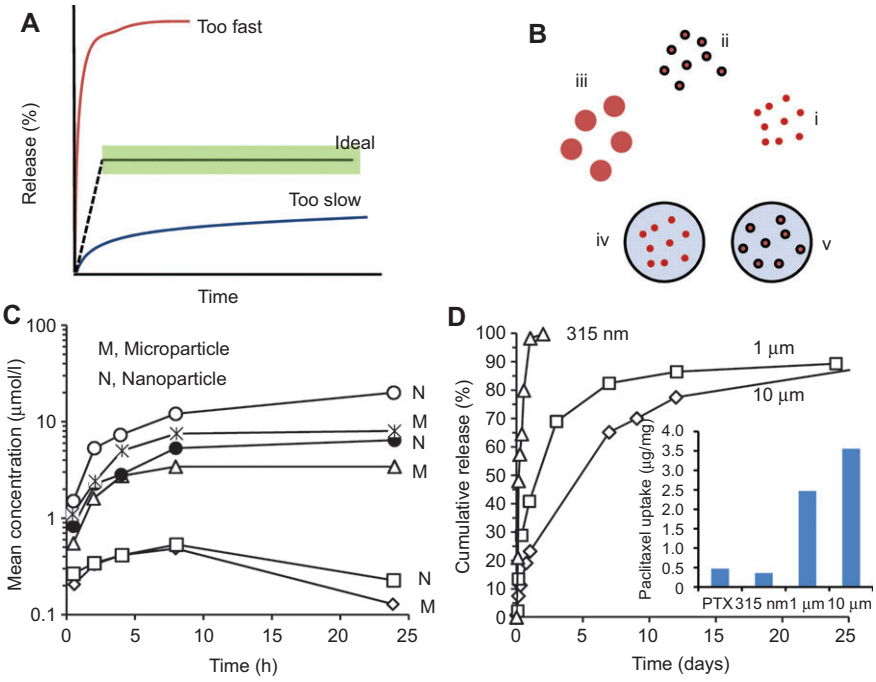

Figure 10 In (A), some extremes of drug release are seen with the ideal release pattern seen marked in green to achieve concentrations in the therapeutic window. (B) (i) Uncoated nanoparticles will typically dissolve quickly with fast systemic clearance, (ii) coating of nanoparticles might stabilize them and control the release to some extent, (iii) uncoated microparticles might be too large for sufficient release, incorporation of (iv) uncoated or (v) coated nanoparticles in coated or uncoated microparticles can stunt release to the desired level while still preserving the advantageous properties of the nanoparticles such as high solubility. (C) Comparative plasma concentration profiles of a drug in nano- or microsuspensions. (D) The comparative release of PTX from solution and particles of various sizes. The 10-µm microparticles showed the highest antitumor efficiency as seen from drug accumulation in the tumor cells [199]. [Copyright (2010) by Elsevier.]

12 Conclusion

The application of nanoscience to improve technology has wide effects on the world, especially on the physical, chemical, and biological technology. The definition of nanotechnology is sometimes quite strict and, depending on the context of the application, takes on different meanings. The boundary of 100 nm is maybe too inflexible for some cases and, for others, again, too lenient. What should be realized is that the marked differences in the material properties are observed on size reduction and is seen once a critical, nanoscale limit is reached.

At the critical nanoscale limit, two of the major deviations from the macroscopic materials are observed. First, the energy transport changes from electron-transport-dominated mechanisms to phonon-dominated mechanisms. Second, the surface-to-volume ratio of the material becomes significantly high so that interfacial and surface properties dominate particle interactions instead of gravity.

Subsequently, the nanoscale energy conversion is different from the macroscopic scale, and we observe changes in the reactivity and responses to ambient conditions such as irradiation and heat. The confinement of the liquids that contain solutes in nanopores can help manipulate and control the nucleation of the solute to selectively crystallize the solute in a certain polymorph or stabilize an amorphous form. The thermal properties such as T_g and T_m are markedly affected and generally show decreases compared to the macroscopic bulk. The solubility and dissolution of the nanosolids are usually improved up to a critical size reduction before small particle agglomeration abolishes this occurrence. For all these properties, the shape of the nanoparticles is also important as the particles are assuming the same size at which the phonon mean free path lengths are seen. The fractal dimensions are also limited to a certain nanoscale range, and therefore, the shape and size should not be separated at the nanoscale. The responsiveness of the nanoparticles to light also renders them unique by the effect of plasmon resonance, facilitating the harnessing of light energy as a localized heating source, which is not possible at the macroscale.

The electrical conductivity of materials is another interesting property that can be modified at the nanoscale. Controllable and guided electrical conductivity is possible by the employment of conductive polymers that is shaped at the nanoscale. Furthermore, these materials can be doped with other particles to extend their functionality or be utilized as structural component of other devices.

Additionally, by modifying the nanoscale structure and texture, the adhesion of carrier systems to biological substrates could also be modified. This modification again points to the multidisciplinary approach to realize nanotechnological applications. The integration and application of the basic physics, chemistry, and biology, all of which cannot exist without the other, is at the forefront to design nanotechnology-based applications. It also difficult to discern which of the properties at the nanoscale contribute most to the deviations observed from the macro- or microscopic scale. It is, therefore, suggested that the interdisciplinary cooperation of these systems is not the only requirement for successful applications but also the hierarchical size-scale organization and integration of these properties.

Drug delivery is one of the multidisciplinary fields that is gaining remarkable interest and benefits from nanotechnology. It is, however, premature to abandon research and application/combination of macro- and microscopic phenomena with the nanodelivery systems. Only with continuous study of all the size-scale regimens will the unique properties at each size scale be realized and integrated. Therefore, the size scale also takes on a multimodal character, or simply put, the observable effects at the large scale can be significantly influenced by tinkering at the nanoscale. It could be envisioned that nanodelivery systems will be fabricated in the future that base their development on the sound knowledge of the physicochemical and biological sciences with consideration of all size hierarchies. The tailoring of the release kinetics at the nanoscale or fabrication of larger carrier systems with nanoscale building blocks will significantly affect the design of drug delivery systems.

Nanotechnology will not solve all our problems, but it is helping us to solve some of them. Nanotechnology is creating the possibility to manipulate the physical, chemical, and biological phenomena at the building-block level. The size scale of the nanoparticles, in most contexts, renders them small enough to interact with large biomolecules such as enzymes and receptors while also allowing the efficient interaction with the smaller molecules. To conclude, nanotechnology has provided us with a means to design particles that can mimic nature and assume multifunctionality at the nanoscale, allowing us to manipulate and adjust the observable, macroscopic world.

Acknowledgements: The authors would like to thank the University of Wisconsin, North-West University, and the National Research Foundation of South Africa for financial support.

Received December 3, 2012; accepted January 2, 2013; previously published online February 16, 2013

References

[1] Balzani V. Nanoscience and nanotechnology: a personal view of a chemist. *Small* 2005, 1, 278–283.
[2] NNI. National Nanotechnology Initiative. Availabe at: http://www.nano.gov. Accessed on 1 September 2012.
[3] Moghimi SM, Kissel T. Particulate nanomedicines. *Adv. Drug Deliv. Rev*. 2006, 58, 1451–1455.
[4] Hughes GA. Nanostructure-mediated drug delivery. *Nanomed. Nanotech. Biol. Med*. 2005, 1, 22–30.
[5] Roco MC. Nanotechnology: convergence with modern biology and medicine. *Curr. Opin. Biotechnol*. 2003, 14, 337–346.
[6] Bogunia-Kubik K, Sugisaka M. From molecular biology to nanotechnology and nanomedicines. *Biosystems* 2002, 65, 123–138.
[7] Xu XH, Brownlow WJ, Kyriacou SV, Wan Q, Viola JJ. Real-time probing of membrane transport in living microbial cells using single nanoparticle optics and living cell imaging. *Biochemistry* 2004, 43, 10400–10413.
[8] Brayden DJ. Controlled release technologies for drug delivery. *Drug Discov. Today* 2003, 8, 976–978.
[9] Ferrari M, Downing G. Medical nanotechnology. Shortening clinical trials and regulatory pathways? *BioDrugs* 2005, 10, 203–210.
[10] Feynman RP. There's plenty of room at the bottom. An invitation to enter a new field of physics. *Eng. Sci*. 1960, 23, 22–36.
[11] Guisbiers G, Shirinyan AS, Wautelet M. The physics of macro-, micro- and nanomaterials. *Phys. Mag*. 2005, 27, 131–141.
[12] Roduner E. Size matters: why nanomaterials are different. *Chem. Soc. Rev*. 2006, 35, 583–592.
[13] Rao CNR, Kulkarni GU, Thomas PJ, Edwards PP. Size-dependent chemistry: properties of nanocrystals. *Chem. Eur. J*. 2002, 8, 28–35.
[14] Yoffe AD. Low-dimensional systems: quantum size effects and electronic properties of semiconductor microcrystallites (zero-dimensional systems) and some quasi-two-dimensional systems. *Adv. Phys*. 1993, 42, 173–266.
[15] Balandin AA. Nanophononics: phonon engineering in nanostructures and nanodevices. *J. Nanosci. Nanotechnol*. 2005, 5, 1015–1022.
[16] Cahill DG, Ford WK, Goodson KE, Mahan GD, Majumdar A, Maris HJ, Merlin R, Phillpot SR. Nanoscale thermal transport. *J. Appl. Phys*. 2003, 93, 793–818.
[17] Shakouri A. Nanoscale thermal transport and microrefrigerators on a chip. *Proc. IEEE* 2006, 94, 1613–1638.
[18] Heeger AJ. Semiconducting and metallic polymers: the fourth generation of polymeric materials. *Synth. Met*. 2001, 125, 23–42.
[19] Long Y, Zhang L, Chen Z, Huang K, Yang Y, Xiao H, Wan M, Jin A, Gu C. Electronic transport in single polyaniline and polypyrolle microtubes. *Phys. Rev. B* 2005, 71, 165412, 1–7.
[20] Feast WJ, Tsibouklis J, Pouwer KL, Groenendaal L, Meijer EW. Synthesis, processing and material properties of conjugated polymers. *Polymer* 1996, 37, 5017–5047.
[21] Spitalsky Z, Tasis D, Papagelis K, Galiotis C. Carbon nanotube composites: chemistry processing and electrical properties. *Prog. Polym. Sci*. 2010, 35, 357–401.
[22] Untereker D, Lyu S, Schley J, Martinez G, Lohstreter L. Maximum conductivity of packed nanoparticles and their polymer composites. *ACS Appl. Mater. Interfaces* 2009, 1, 97–101.
[23] Knite M, Teteris V, Polyakov B, Erts D. Electric and elastic properties of conductive polymeric nanocomposites on macro- and nanoscales. *Mater. Sci. Eng. C* 2002, 19, 15–19.
[24] Heeger AJ. Charge transfer in conducting polymers. *Faraday Discuss*. 1989, 88, 203–211.
[25] Heeger AJ. Semiconducting polymers: the third generation. *Chem. Soc. Rev*. 2010, 39, 2354–2371.
[26] Nordén B, Krutmeijer E. The Nobel Prize in Chemistry, 2000: Conductive polymers. Availabe at: http://nobelprize.org/nobel_prizes/chemistry/laureates/2000/chemadv.pdf. Accessed on 1 September 2012.
[27] Brezoi DV, Ion RM. Phase evolution induced by polypyrolle in iron oxide-polypyrolle nanocomposite. *Sens. Actuators B* 2005, 109, 171–175.
[28] Long, YZ, Chen, Z, Gum, C, Wan M, Duvail, JC, Liu Z, Ringer, SP. A review on electronic properties of individual and conducting polymer nanotubes and nanowires. In *Nanowires Science and Technology*, Lupu, N, Ed., INTECH: Croatia, 2010, pp. 223–242.
[29] Jin J, Wang Q, Haque MA. Length-scale effects on electrical and thermal transport in polyaniline thin films. *Org. Electron*. 2010, 11, 29–35.
[30] Li C, Thostenson ET, Chou TW. Effect of nanotube waviness on the electrical conductivity of carbon nanotube-based composites. *Compos. Sci. Technol*. 2008, 68, 1445–1452.
[31] Zeng Y, Liu P, Du J, Zhao L, Ajayan PM, Cheng HM. Increasing the electrical conductivity of carbon nanotube/polymer composites by using weak nanotube-polymer interaction. *Carbon* 2010, 48, 3551–3558.
[32] Takeda T, Shindo Y, Kuronuma Y, Narita F. Modeling and characterization of the electrical conductivity of carbon-based polymer composites. *Polymer* 2011, 52, 3852–3856.
[33] Yoshino K, Kawagishi S, Lee S, Nakayama K, Take H, Kaji H. Electrical and optical properties of conducting polymer and carbons in nano-scale periodic structure and their intercalation effects. *Mol. Cryst. Liq. Cryst. Sci. Technol. A* 2000, 341, 485–490.
[34] Geetha S, Rao CRK, Vijayan M, Trivedi DC. Biosensing and drug delivery by polypyrrole. *Anal. Chim. Acta* 2006, 568, 119–125.
[35] Ravichandran R, Sundarrajan S, Venugopal JR, Mukherjee S, Ramakrishna S. Applications of conducting polymers and their issues in biomedical engineering, *J. R. Soc. Interface* 2010, 7, S559–S579.
[36] Guimard NK, Gomez N, Schmidt CE. Conducting polymers in biomedical engineering. *Prog. Polym. Sci*. 2007, 32, 876–921.
[37] Wadhwa R, Lagenaur, CF, Cui XT. Electrochemically controlled release from conducting polymer coated electrode. *J. Control. Release* 2006, 110, 531–541.
[38] Abidian MZ, Kim DH, Martin DC. Conductive-polymer nanotubes for controlled drug release. *Adv. Mater*. 2006, 17, 405–409.
[39] Luo X, Cui XT. Electrochemically controlled release based on nanoporous conducting polymers. *Electrochem. Commun*. 2009, 11, 402–404.
[40] Sun Y, Xia Y. Gold and silver nanoparticles: a class of chromophores with colors tunable in the range from 400 to 750 nm. *Analyst* 2003, 128, 686–691.

[41] Nobile C, Kudera S, Fiore A, Carbone L, Chilla G, Kipp T, Heitmann D, Cingolani R, Manna L, Krahne R. Confinement effects on optical phonons in spherical, rod-, and tetrapod-shaped nanocrystals detected by Raman spectroscopy. *Phys. Stat. Solidi A: Appl. Mater. Sci.* 2007, 204, 483–486.
[42] Xu X, Cortie MB. Shape change and color gamut in gold nanorods, dumbbells, and dog bones. *Adv. Funct. Mater.* 2006, 16, 2170–2176.
[43] He YQ, Liu SP, Kong L, Liu ZF. A study on the sizes and concentrations of gold nanoparticles by spectra of absorption, resonance Rayleigh scattering and resonance non-linear scattering. *Spectrochim. Acta A Mol. Biomol. Spectrosc.* 2005, 61, 2861–2866.
[44] Hu M, Chen J, Li ZY, Au L, Hartland GV, Li X, Marquez M, Xia Y. Gold nanostructures: engineering their plasmonic properties for biomedical applications. *Chem. Soc. Rev.* 2006, 35, 1084–1094.
[45] Hirsch LR, Gobon AM, Lowery AR, Tam F, Drezek RA, Halas NJ, West JL. Metal nanoshells. *Ann. Biomed. Eng.* 2006, 34, 15–22.
[46] Aizpurua J, Hanarp P, Sutherland DS, Käll M, Bryant GW, De Abajo FJG. Optical properties of gold nanorings. *Phys. Rev. Lett.* 2003, 90, 057401-1–057401-5.
[47] Haes AJ, Stuart DA, Nie S, van Duyne RP. Using solution-phase nanoparticles, surface-confined nanoparticles arrays and single nanoparticles as biological sensing platforms. *J. Fluoresc.* 2004, 14, 355–367.
[48] Loo C, Lin A, Hirsch L, Lee MH, Barton J, Halas N, West J, Drezek R. Nanoshell-enabled photonics-based imaging and therapy of cancer. *Technol. Cancer Res. Treat.* 2004, 3, 33–40.
[49] Govorov AO, Richardson HH. Generating heat with metal nanoparticles. *Nano Today* 2007, 2, 30–38.
[50] Liao H, Nehl CL, Hafner JH. Biomedical applications of plasmon resonant metal nanoparticles. *Nanotechnology* 2006, 1, 201–208.
[51] You J, Zhang G, Li C. Exceptionally high payload of doxorubicin in hollow gold nanospheres for near-infrared light-triggered drug release. *ACS Nano* 2010, 4, 1033–1041.
[52] Quenten M. The color of finely dispersed nanoparticles. *Appl. Phys. B: Lasers Opt.* 2001, 73, 317–326.
[53] Jain PK, El-Sayed IH, El-Sayed MS. Au nanoparticles target cancer. *Nano Today* 2007, 2, 18–29.
[54] Hatta I. Thermal characteristics in a nanometer scale. *J. Therm. Anal. Calorim.* 2002, 69, 717–725.
[55] Chen G. Particularities of heat conduction in nanostructures. *J. Nanopart. Res.* 2000, 2, 199–204.
[56] Michel M, Gemmer J, Mahler G. Microscopic quantum mechanical foundation of Fouriers's Law. *Int. J. Mod. Phys. B* 2006, 1, 1–30.
[57] Lepri S, Livi R, Politi A. Thermal conduction in classical low-dimensional lattices. *Phys. Rep.* 2003, 377, 1–80.
[58] Kim W, Wang R, Majumdar A. Nanostructuring expands thermal limits. *Nano Today* 2007, 2, 40–47.
[59] Tien CL, Chen G. Challenges in microscale conductive and radiative heat transfer. *J. Heat Trans.* 1994, 116, 799–807.
[60] Cenian A, Gabriel H. Ballistic energy transfer in dielectric Ar crystals. *J. Phys.: Condens. Matter* 2001, 13, 4323–4339.
[61] Chen G. Ballistic-diffusive equations for transient heat conduction from nano to macroscales. *J. Heat Trans.* 2002, 124, 320–328.
[62] Gomes CJ, Madrid M, Goicochea JV, Amon CH. In-plane and out-of-plane thermal conductivity of silicon thin films predicted by molecular dynamics. *J. Heat Trans.* 2006, 128, 1114–1121.
[63] Chen G. Nonlocal and nonequilibrium heat conduction in the vicinity of nanoparticles. *J. Heat Transfer* 1996, 118, 539–545.
[64] Rieger J, Horner D. Organic nanoparticles in the aqueous phase – theory, experiment, and use. *Angew. Chem. Int. Ed. Engl.* 2001, 40, 4330–4361.
[65] Diao Y, Helgeson ME, Myerson AS, Hatton TA, Doyle PS, Trout BL. Controlled nucleation from solution using polymer microgels. *J. Am. Chem. Soc.* 2011, 133, 3756–3759.
[66] Diao Y, Myerson AS, Hatton TA, Trout BL. Surface design for controlled crystallization: the role of surface chemistry and nanoscale pores in heterogeneous nucleation. *Langmuir* 2011, 27, 5324–5334.
[67] Ha JM, Wolf JH, Hillmyer MA, Ward MD. Polymorph selection under nanoscopic confinement. *J. Am. Chem. Soc.* 2004, 126, 3382–3383.
[68] Oxtoby DW. Nucleation of first-order phase transitions. *Acc. Chem. Res.* 1998, 31, 91–97.
[69] Kim K, Centrone A, Hatton TA, Myerson AS. Polymorphism control of nanosized glycine crystals on engineered surfaces. *Cryst. Eng. Comm.* 2011, 13, 1127–1131.
[70] Mannsfeld SCB, Briseno AL, Liu S, Reese C, Roberts ME, Bao Z. Selective nucleation of organic single crystals from vapor phase on nanoscopically rough surfaces. *Adv. Funct. Mater.* 2007, 17, 3545–3553.
[71] Tomalia DA, Naylor AM, Goddard WA. Starburst dendrimers: molecular-level control of size, shape, surface chemistry, topology, and flexibility from atoms to macroscopic matter. *Angew. Chem. Int. Ed.* 1990, 29, 138–175.
[72] Naka K, Tanaka Y, Chujo Y. Effect of anionic starburst dendrimers on the crystallization of $CaCO_3$ in aqueous solution: size control of spherical vaterite particles. *Langmuir* 2002, 18, 3655–3658.
[73] Wu T, Sun Y, Li N, De Villiers MM, Yu L. Inhibiting surface crystallization of amorphous indomethacin by nanocoating. *Langmuir* 2007, 23, 5148–5153.
[74] Zhang Z, Zhao M, Jiang Q. Glass transition thermodynamics of organic nanoparticles. *Physica B* 2001, 293, 232–236.
[75] Jiang Q, Shi HX, Li JC. Finite size effect on glass transition temperatures. *Thin Solid Films* 1999, 354, 283–286.
[76] Koh YP, McKenna GB, Simon SL. Calorimetric glass transition temperature and absolute heat capacity of polystyrene ultrathin films. *J. Polym. Sci. Part B, Polym. Phys.* 2006, 44, 3518–3527.
[77] Bares J. Glass transition of the polymer microphase. *Macromolecules* 1975, 8, 244–246.
[78] Fox TG, Flory PJ. Second-order transition temperatures and related properties of polystyrene. I. Influence of the molecular weight. *J. Appl. Phys.* 1950, 21, 581–591.
[79] Jackson CL, McKenna GB. Vitrification and crystallization of organic liquids confined to nanoscale pores. *Chem. Mater.* 1996, 8, 2128–2137.
[80] MacFarlane DR, Angell CA. An emulsion technique for the study of marginal glass formation in molecular liquids. *J. Phys. Chem.* 1982, 86, 1927–1930.
[81] Alba C, Busse LE, List DJ, Angell CA. Thermodynamic aspects of the vitrification of toluene, and xylene isomers, and the fragility of liquid hydrocarbons. *J. Chem. Phys.* 1990, 92, 617–624.

[82] Xiong XY, Tam KC, Gan LH. Release kinetics of hydrophobic and hydrophilic model drugs from pluronic F127/poly(lactic acid) nanoparticles. *J. Control. Release* 2005, 103, 73–82.
[83] Missirlis D, Hubbell JA, Tirelli N. Thermally-induced glass formation from hydrogel nanoparticles. *Soft Matter* 2006, 2, 1067–1075.
[84] Jiang Q, Yang CC, Li JC. Melting enthalpy depression of nanocrystals. *Mater. Lett.* 2002, 56, 1019–1021.
[85] Liang LH, Zhao M, Jiang Q. Melting enthalpy depression of nanocrystals based on surface effect. *J. Mater. Sci. Lett.* 2002, 21, 1843–1845.
[86] Shrivastava KN. Melting temperature, Brillouin shift, and density of states of states of nanocrystals. *Nano Lett.* 2002, 2, 519–523.
[87] Xue Y, Zhao Q, Luan C. The thermodynamic relations between the melting point and the size of crystals. *J. Colloid Interface Sci.* 2001, 243, 388–390.
[88] Qi WH. Size effect on melting temperature of nanosolids. *Physica B* 2005, 368, 46–50.
[89] Guinea F, Rose JR, Smith JR, Ferrante J. Scaling relations in the equation of state, thermal expansion, and melting of metals. *Appl. Phys. Lett.* 1984, 44, 53–55.
[90] Buffat P, Borel JP. Size effect on the melting temperature of gold particles. *Phys. Rev. A: At. Mol. Opt. Phys.* 1976, 13, 2287–2298.
[91] Guisbiers G, Wautelet M. Size, shape and stress effects on the melting temperature of nano-polyhedral grains on a substrate. *Nanotechnology* 2006, 17, 2008–2011.
[92] Wang XW, Fei GT, Zheng K, Jin Z, Zhang LD. Size-dependent melting behavior of Zn nanowire arrays. *Appl. Phys. Lett.* 2006, 88, 173114-1–173114-3.
[93] Zhang Z, Li JC, Jiang Q. Modelling for size-dependent and dimension-dependent melting of nanocrystals. *J. Phys. D: Appl. Phys.* 2000, 33, 2653–2656.
[94] Wautelet M, Dauchot JP, Hecq M. Size effects on the phase diagrams of nanoparticles of various shapes. *Mater. Sci. Eng. C* 2003, 23, 187–190.
[95] Wautelet M. On the shape dependence of the melting temperature of small particles. *Phys. Lett. A* 1998, 246, 341–342.
[96] Sun CQ, Li CM, Bai HL, Jiang EY. Melting point oscillation of a solid over the whole range of sizes. *Nanotechnology* 2005, 16, 1290–1293.
[97] Jiang Q, Shi HX, Zhao M. Melting thermodynamics of organic nanocrystals. *J. Chem. Phys.* 1999, 111, 2176–2180.
[98] Mottet C, Rossi G, Baletto F, Ferrando R. Single impurity effect on the melting of nanoclusters. *Phys. Rev. Lett.* 2005, 95, 035501-1–035501-4.
[99] Bergese P, Colombo I, Gervasoni D, Depero LE. Melting of nanostructured drugs embedded into a polymeric matrix. *J. Phys. Chem. B* 2004, 108, 15488–15493.
[100] Shirinyan AS, Wautelet M. Phase separation in nanoparticles. *Nanotechnology* 2004, 15, 1720–1731.
[101] Shirinyan AS, Gusak AM, Wautelet M. Phase diagrams versus diagram of solubility: what is the difference for nanosystems? *Acta Mater.* 2005, 53, 5025–5032.
[102] Dalnoki-Veress K, Forrest JA, Murray C, Cigault C, Dutcher JR. Molecular weight dependence of reductions in the glass transition temperature of thin, freely standing polymer films. *Phys. Rev. E: Stat., Nonlinear, Soft Matter Phys.* 2001, 031801-1–031801-10.
[103] Mihranyan A, Strømme M. Solubility of fractal nanoparticles. *Surf. Sci.* 2007, 601, 315–319.
[104] Hildebrandt JH. Solubility. XII. Regular solutions. *J. Am. Chem. Soc.* 1929, 51, 66–80.
[105] Yalkowsky SH, Valvani SC. Solubility and partitioning I: solubility of nonelectrolytes in water. *J. Pharm. Sci.* 1980, 69, 912–922.
[106] Amidon GL, Yalkowsky SH, Leung S. Solubility of nonelectrolytes in polar solvents II: solubility of aliphatic alcohols in water. *J. Pharm. Sci.* 1974, 63, 1858–1866.
[107] Berg JC. *An Introduction to Interfaces and Colloids. The Bridge to Nanoscience*. World Scientific Publishing: New Jersey, 2010.
[108] Bisrat M, Nyström C. Physicochemical aspects of drug release. VIII. The relation between particle size and surface specific dissolution rate in agitated suspensions. *Int. J. Pharm.* 1988, 47, 223–231.
[109] Galvin KP. A conceptually simple derivation of the Kelvin equation. *Chem. Eng. Sci.* 2005, 60, 4659–4660.
[110] Nanda KK, Maisels A, Kruis FE, Fissan H, Stappert S. Higher surface energy of free nanoparticles. *Phys. Rev. Lett.* 2003, 91, 106102-1–106102-4.
[111] Smolen VF, Kildsig DO. Vapor pressure and solubility of small particles. *Am. J. Pharm. Ed.* 1967, 31, 512–514.
[112] Ouyang G, Tan X, Wang CX, Yang GW. Solid solubility limit in alloying nanoparticles. *Nanotechnology* 2006, 17, 4257–4262.
[113] Tang R, Wang L, Nancollas GH. Size-effects in the dissolution of hydroxyapatite: an understanding of biological demineralization. *J. Mater. Chem.* 2004, 14, 2341–2346.
[114] Kipp JE. The role of solid nanoparticle technology in the parenteral delivery of poorly water-soluble drugs. *Int. J. Pharm.* 2004, 284, 109–122.
[115] Noyes AA, Whitney WR. The rate of solution of solid substances in their own solutions. *J. Am. Chem. Soc.* 1897, 19, 930–934.
[116] Hixson AW, Crowell JH. Dependence of reaction velocity upon surface and agitation. I. Theoretical consideration. *Ind. Eng. Chem.* 1931, 23, 923–931.
[117] Tinke AP, Vanhoutte K, de Maesschalck R, Verheyen S, de Winter H. A new approach in the prediction of the dissolution behavior of suspended particles by means of their particle size distribution. *J. Pharm. Biomed. Anal.* 2005, 39, 900–907.
[118] Anderberg EK, Bisrat M, Nyström C. Physicochemical aspects of drug release. VII The effect of surfactant concentration and drug particle size on solubility and dissolution rate of felodipine, a sparingly soluble drug. *Int. J. Pharm.* 1988, 47, 67–77.
[119] Galli C. Experimental determination of the diffusion boundary layer width of micron and submicron particles. *Int. J. Pharm.* 2006, 313, 114–122.
[120] Heywood H. Particle shape coefficients. *J. Imp. College Chem. Soc.* 1954, 8, 25–33.
[121] Mosharraf M, Nytsröm C. Effect of particle size and shape on the surface specific dissolution rate of micronized practically insoluble drugs. *Int. J. Pharm.* 1995, 122, 35–47.
[122] Zhang H, Gilbert B, Huang F, Banfield JF. Water-driven structure transition in nanoparticles at room temperature. *Nature* 2003, 424, 1025–1029.
[123] Sdobnyakov NY, Samsonov VM. On the size dependence of surface tension in the temperature range from melting point to critical point. *Cent. Eur. J. Phys.* 2005, 3, 247–257.

[124] Powell C, Fenwick N, Bresme F, Quirke N. Wetting of nanoparticles and nanoparticle arrays. *Colloids Surf. A* 2002, 206, 241–251.
[125] Liu Y, Chen X, Xin JH. Super-hydorphobic surface from a simple coating: a bionic nanoengineering approach. *Nanotechnology* 2006, 17, 3259–3263.
[126] Crisp MW, Tucker CJ, Rogers TL, Williams RO, Johnston KP. Turbidimetric measurement and prediction of dissolution rates of poorly soluble drug nanoparticles. *J. Control. Release* 2007, 117, 351–359.
[127] Bisrat M, Anderberg EK, Barnett MI, Nyström C. Physico-chemical aspects of drug release. XV. Investigation of diffusional transport in dissolution of suspended, sparingly soluble drugs. *Int. J. Pharm*. 1992, 80, 191–201.
[128] Aharoni C. The solid-liquid interface in capillary condensation. Sorption of water by active carbons. *Langmuir* 1997, 13, 1270–1273.
[129] Aharoni C. Effect of the energy of adsorption at the pore wall surface on capillary condensation. *Langmuir* 2002, 18, 7441–7446.
[130] Aharoni C. Adsoprtion and condensation in pores. *Langmuir* 1998, 14, 3339–3342.
[131] Dobruskin VK. Correlation between saturation pressures and dimensions of nanoparticles. Are the fundamental equations really fair? *Langmuir* 2003, 19, 4004–4013.
[132] Germain J, Hradil J, Fréchet JMJ, Svec F. High surface area nanoporous polymers for reversible hydrogen storage. *Chem. Mater*. 2006, 18, 4430–4435.
[133] Aranovich GL, Donohue MD. The role of adsorption compression in nanocapillaries. *J. Colloid Interface Sci*. 2005, 292, 202–209.
[134] Brovchenko I, Geiger A, Oleinikova A. Water in nanopores. I. Coexistence curves from Gibbs ensemble Monte Carlo simulations. *J. Chem. Phys*. 2004, 120, 1958–1972.
[135] Ravikovitch PI, Neimark AV. Experimental confirmation of different mechanisms of evaporation from ink-bottle type pores: equilibrium, pore blocking, and cavitation. *Langmuir* 2002, 18, 9830–9837.
[136] Stillinger FH. Structure in aqueous solutions of nonpolar solutes from the standpoint of scaled-particle theory. *J. Sol. Chem*. 1973, 2, 141–158.
[137] Luzar A. Activation barrier scaling for the spontaneous evaporation of confined water. *J. Phys. Chem. B* 2004, 108, 19859–19866.
[138] Lum K, Luzar A. Pathway to surface-induced phase transition of a confined fluid. *Phys. Rev. E: Stat. Nonlinear Soft Matter Phys*. 1997, 56, R6283–R6286.
[139] Leung K, Luzar A, Bratko D. Dynamics of capillary drying in water. *Phys. Rev. Lett*. 2003, 90, 065502-1–065502-4.
[140] Maeda N, Israelachvili JN. Nanoscale mechanisms of evaporation, condensation and nucleation in confined geometries. *J. Phys. Chem. B* 2002, 106, 3534–3537.
[141] Beckstein O, Biggin PC, Sansom MSP. A hydrophobic gating mechanism for nanopores. *J. Phys. Chem. B* 2001, 105, 12902–12905.
[142] Sansom MSP, Biggin PC. Water at the nanoscale. *Nature* 2001, 414, 156–159.
[143] Beckstein O, Tai K, Sansom MSP. Not ions alone: barriers to ion permeation in nanopores and channels. *J. Am. Chem. Soc*. 2004, 126, 14694–14695.
[144] Allen R, Melchionna S, Hansen JP. Intermittent permeation of cylindrical nanopores by water. *Phys. Rev. Lett*. 2002, 89, 175502-1-4.
[145] Allen R, Hansen JP, Melchionna S. Molecular dynamics investigation of water permeation through nanopores. *J. Chem. Phys*. 2003, 119, 3905–3919.
[146] Truskett TM, Debenedetti PG, Torquato S. Thermodynamic implications of confinement for a waterlike fluid. *J. Chem. Phys*. 2001, 114, 2401–2418.
[147] Celestini F. Capillary condensation within nanopores of various geometries. *Phys. Lett. A* 1997, 228, 84–90.
[148] Ramírez P, Mafé S, Alcaraz A, Cervera J. Modeling the pH-switchable ion transport and selectivity in nanopores membranes with fixed charges. *J. Phys. Chem. B* 2003, 107, 13178–13187.
[149] Leung K, Rempe SB, Lorenz CD. Salt permeation and exclusion in hydroxylated and functionalized silica pores. *Phys. Rev. Lett*. 2006, 96, 095504-1–095504-1-4.
[150] Asefa T, Otuonye AN, Wang G, Blair EA, Vathyam R, Denton K. Controlling adsorption of drug and small molecules by organic functionalization of mesoporous materials. *Adsorption* 2009, 15, 287–299.
[151] Vathyaman R, Wondimu E, Das S, Zhang C, Hayes S, Tao Z, Asefa T. Improving the adsorption and release capacity of organic-functionalized mesoporous materials to drug molecules with temperature and synthetic methods. *J. Phys. Chem. C* 2011, 115, 13135–13150.
[152] Brás AR, Merino EG, Neves PD, Fronseca IM, Dioníso M, Schönhals A, Correia NT. Amorphous ibuprofen confined in nanostructured silica materials: a dynamical approach. *J. Phys. Chem. C* 2011, 115, 4616–4623.
[153] Kim MH, Ayral A, Park CB, Choy JH, Oh JM. Diffusion control of porous membrane by modifying pore properties. *J. Nanosci. Nanotechnol*. 11, 1656–1659.
[154] Berg MC, Zhai L, Cohen RE, Rubner MF. Controlled drug release from porous polyelectrolyte multilayers. *Biomacromolecules* 2006, 7, 357–364.
[155] Vaccari L, Canton D, Zaffaroni N, Villa R, Tormen M, di Fabrizio E. Porous silicon as carrier for controlled delivery of doxorubicin anticancer agent. *Microelectron. Eng*. 2006, 83, 1598–1601.
[156] Muhammad F, Guo M, Qi W, Sun F, Wang A, Guo Y, Zhu G. pH-triggered controlled drug release from mesoporous silica nanoparticles via intracellular dissolution of ZnO nanolids. *J. Am. Chem. Soc*. 2011, 133, 8778–8781.
[157] Hong Y, Chen X, Jing X, Fan H, Guo B, Gu Z, Zhang X. Preparation, bioactivity, and drug release of hierarchical nanoporous bioactive glass ultrathin fibers. *Adv. Mater*. 2010, 22, 754–758.
[158] Ambrogi V, Perioli L, Marmottini F, Accorso O, Cinzia P, Ricci M, Rossi C. Role of mesoporous silicates on carbamazepine dissolution rate enhancement. *Microporous Mesoporous Mater*. 2008, 113, 445–452.
[159] Rengarajan GT, Enke D, Steinhart M, Beiner M. Stabilization of the amorphous state of pharmaceuticals in nanopores. *J. Mater. Chem*. 2008, 18, 2537–2539.
[160] Lo KH, Chen MC, Ho RM, Sung HS. Pore-filling nanoporous templates from degradable block copolymers for nanoscale drug delivery. *ACS Nano* 2009, 3, 2660–2666.
[161] Signoretto M, Ghedini E, Nichele V, Pinna F, Crocellà V, Cerrato G. Effect of textural properties on the drug delivery

behavior of nanoporous TiO_2 matrices. *Microporous Mesoporous Mater*. 2011, 139, 189–196.
[162] Chaban VV, Prezhdo OV. Water boiling inside carbon nanotubes: toward efficient drug releae. *ACS Nano* 2011, 5, 5647–5655.
[163] Alleman E, Gurny R, Doelker E. Drug-loaded nanoparticles. Preparation methods and targeting issues. *Eur. J. Pharm. Biopharm* 1993, 39, 173–191.
[164] Chorny M, Fishbein I, Haim D, Golomb G. Study of the drug release mechanism from yrphostin AG-1295-loaded nanospheres by in situ and external sink methods. *J. Control. Release* 2002, 83, 401–414.
[165] Lecaroz C, Gamazo C, Renedo MJ, Blanco-Prieto MJ. Biodegradable micro- and nanoparticles as long-term delivery vehicles for gentamicin. *J. Microencapsul.* 2006, 23, 782–789.
[166] Beck RCR, Pohlmann AR, Guterres SS. Nanoparticle-coated microparticles: preparation and characterization. *J. Microencapsul.* 2004, 21, 499–512.
[167] Bapat N, Boroujerdi M. Uptake capacity and adsorption isotherms of doxorubicin on polymeric nanoparticles: effects of methods of preparation. *Drug Dev. Ind. Pharm*. 1992, 18, 65–77.
[168] Illum L, Khan MA, Mak E, Davis SS. Evaluation of carrier capacity and release characteristics of poly(butyl 2-cyanoacrylate) nanoparticles. *Int. J. Pharm*. 1986, 30, 17–28.
[169] Lopes E, Pohlmann AR, Bassani V, Guterres SS. Polymeric colloidal systems containing ethionamide: preparation and physic-chemical characterization. *Pharmazie* 2000, 55, 527–530.
[170] Soppimath KS, Aminabhavi TM, Kulkarni AR, Rudzinski WE. Biodegradable polymeric nanoparticles as drug delivery devices. *J. Control. Release* 2001, 70, 1–20.
[171] Opanasopit P, Ngawhirunpat T, Chaidedgumjorn A, Rojanarata T, Apirakaramwong A, Phongying S, Choochottiros C, Chirachanchai S. Incorporation of camptothecin into *N*-phtaloyl chitosan chitosan-*g*-mPEG self-assembly micellar systems. *Eur. J. Pharm. Biopharm*. 2006, 64, 269–276.
[172] Bhattarai N, Ramay HR, Chou SH, Zhang M. Chitosan and lactic acid-grafted chitosan nanoparticles as carriers for prolonged drug delivery. *Int. J. Pharm*. 2006, 1, 181–187.
[173] Govender T, Riley T, Ehtezazi T, Garnett MC, Stolnik S, Illum L, Davis SS. Defining the drug incorporation properties of PLA-PEG nanoparticles. *Int. J. Pharm*. 2000, 199, 95–110.
[174] Huo Q, Liu J, Wang LQ, Jiang Y, Lambert TN, Fang E. A new class of silica cross-linked micellar core-shell nanoparticles. *J. Am. Chem. Soc*. 2006, 128, 6447–6453.
[175] Jiang B, Hu L, Gao C, Jiacong S. Ibuprofen-loaded nanoparticles prepared by a co-precipitation methods and their release properties. *Int. J. Pharm*. 2005, 304, 220–230.
[176] Pandey R, Ahmad Z, Sharma S, Khuller GK. Nano-encapsulation of azole antifungals: potential applications to improve oral drug delivery. *Int. J. Pharm*. 2005, 301, 268–276.
[177] Patri AK, Kukowska-Latallo JF, Baker JR. Targeted drug delivery with dendrimers: comparison of the release kinetics of covalently conjugated drug and non-covalent drug inclusion complex. *Adv. Drug Deliv. Rev*. 2005, 57, 2203–2214.
[178] Kolhe P, Misra E, Kannan RM, Kannan S, Lieh-Lai M. Drug complexation, in vitro release and cellular entry of dendrimers and hyperbranched polymers. *Int. J. Pharm*. 2003, 259, 143–160.
[179] Govender T, Stolnik S, Garnett MC, Illum L, Davis SS. PLGA nanoparticles prepared by nanoprecipitation: drug loading and release studies of a water soluble drug. *J. Control. Release* 1999, 57, 171–185.
[180] Gaber NN, Darwis Y, Peh KK, Tan YTF. Characterization of polymeric micelles for pulmonary delivery of beclomethasone dipropionate. *J. Nanosci. Nanotechnol*. 2006, 6, 3095–3101.
[181] Higuchi T. Mechanism of sustained-action medication. Theoretical analysis of rate of release of solid drugs dispersed in solid matrices. *J. Pharm. Sci*. 1963, 52, 1145–1149.
[182] Zhang J, Xiang L, Xiao J, Qiu L, Yan L, Xiao H, Yan MQJ, Yi J, Zhu KJ. Indomethacin-loaded polymeric nanocarriers based on amphiphilic polyphosphazenes with poly (*N*-isopropylacrylamide) and ethyl tryptophan as side groups: preparation, in vitro and in vivo evaluation. *J. Control. Release* 2006, 116, 322–329.
[183] Guy RH, Hadgraft J, Kellaway IW, Taylor JM. Calculations of drug release from spherical particles. *Int. J. Pharm*. 1982, 11, 199–207.
[184] Ritger PL, Peppas NA. A simple equation for description of solute release. 1. Fickian and non-Fickian release from non-swellable devices in the form of slabs, spheres, cylinders or disks. *J. Control. Release* 1987, 5, 23–36.
[185] Ritger PL, Peppas NA. A simple equation for description of solute release. II. Fickian and anomalous release from swellable devices. *J. Control. Release* 1987, 5, 37–42.
[186] Leo E, Scatturin A, Vighi E, Dalpiaz A. Polymeic nanoparticles as drug controlled release systems: a new formulation strategy for drugs with small or large molecular weight. *J. Nanosci. Nanotech*. 2006, 6, 3070–3079.
[187] Siepmann J, Göpferich A. Mathematical modeling of bioerodible, polymeric drug delivery systems. *Adv. Drug Deliv. Rev*. 2001, 48, 229–247.
[188] Siepmann J, Faisant N, Benoit JP. A new mathematical model quantifying drug release from bioerodible microparticles using Monte Carlo simulations. *Pharm. Res*. 2002, 19, 1885–1893.
[189] Panyam J, Dali MM, Sahoo SK, Ma W, Chakravarthi SS, Amidon GL, Levy RJ, Labhasetwar V. Polymer degradation and in vitro release of a model protein from poly(D,L-lactide-*co*-glycolide) nano- and microparticles. *J. Control. Release* 2003, 92, 173–187.
[190] Jo YS, Kim MC, Kyung D, Kim CJ, Jeong YK, Kim KJ, Muhammed M. Mathematical modeling on the controlled-release of indomethacin-encapsulated poly(lactic acid-*co*-ethylene oxide) nanospheres. *Nanotechnology*. 2004, 15, 1186–1194.
[191] Polakovič M, Gorner T, Gref R, Dellacherie E. Lidocaine loaded biodegradable nanospheres. II. Modelling of drug release. *J. Control. Release* 1999, 60, 169–177.
[192] Zur Mühlen A, Mehnert W. Drug release and release mechanism of prednisolone loaded solid lipid nanoparticles. *Pharmazie* 1998, 53, 552–555.
[193] Sukhorukov GB, Fery A, Brumen M, Möhwald H. Physical chemistry of encapsulation and release. *Phys. Chem. Chem. Phys*. 2004, 6, 4078–4089.
[194] De Geest BG, Sanders NN, Sukhorukov GB, Demeester J, De Smedt SC. Release mechanisms for polyelectrolyte capsules. *Chem. Soc. Rev*. 2007, 36, 636–649.

[195] Johnston APR, Cortez C, Angelatos AS, Caruso F. Layer-by-layer engineered capsules and their applications. *Curr. Opin. Colloid Interface Sci.* 2006, 203–209.
[196] Redhead HM, Davis SS, Illum L. Drug delivery in poly(lactide-co-glycolide) nanoparticles surface modified with poloxamer 407 and poloxamine 908: in vitro characterization and in vivo evaluation. *J. Control. Release* 2001, 70, 353–363.
[197] Gref R, Quellec P, Sanchez A, Calvo P, Dellacherie E, Alonso MJ. Development and characterization of CyA-loaded poly(lactic acid)-poly(ethylene glycol) PEG micro- and nanoparticles. Comparison with conventional PLA particulate carriers. *Eur. J. Pharm. Biopharm.* 2001, 51, 111–118.
[198] Lu XY, Zhang Y, Wang L. Preparation and in vitro drug-release behavior of 5-fluorouracil-loaded poly(hydroxybutyrate-*co*-hydroxyhexanoate) nanoparticles and nanoparticles. *J. Appl. Polym. Sci.* 2010, 116, 2944–2950.
[199] Chakravarthi SS, De S, Miller DW, Robinson DH. Comparison of anti-tumor efficacy of paclitaxel delivered in nano- and microparticles. *Int. J. Pharm.* 2010, 383, 37–44.
[200] Parajó Y, d'Angelo I, Horváth A, Vantus T, György K, Welle A, Garcia-Fuentes M, Alonso MJ. PLGA:poloxamer blend micro- and nanoparticles as controlled release systems for synthetic proangiogenic factors. *Eur. J. Pharm. Sci.* 2010, 41, 644–649.
[201] Miao ZM, Cheng SX, Zhang XZ, Zhuo RX. Study on drug release behaviors of poly-α,β-[*N*-(2-hydroxyethyl)-L-aspartamide]-*g*-poly(ε-caprolactone) nano- and microparticles. *Biomacromolecules* 2006, 7, 2020–2026.
[202] Hasan AS, Socha M, Lamprecht A, Ghazouani FE, Sapin A, Hoffman M, Maincent P, Ubrich N. Effect of the microencapsulation of nanoparticles on the reduction of burst release. *Int. J. Pharm.* 2007, 344, 53–61.
[203] Sigfridsson K, Nordmark A, Theilig S, Lindahl A. A formulation comparison between micro- and nanosuspensions: the importance of particle size for absorption of a model compound, following repeated oral administration to rats during early development. *Drug Dev. Ind. Pharm.* 2011, 37, 185–192.
[204] Tsai M, Lu Z, Wang J, Yeh TK, Wientjies MG, Au JLS. Effects of carrier on disposition and antitumor activity of intraperitoneal paclitaxel. *Pharm. Res.* 2007, 24, 1691–1701.

Daniel P. Otto is a Postdoctoral Researcher from the Catalysis and Synthesis Research Group, Chemical Resource Beneficiation Research Focus Area, Faculty of Natural Sciences, North-West University, South Africa. He completed part of his postdoctoral study working at the School of Pharmacy at the University of Wisconsin. His research interests are, in general, nanotechnological pharmaceutics and, in particular, designing drug delivery systems for controlled and targeted delivery using LbL self-assembly. He is the coauthor of 10 papers in the field of nanosized drug delivery systems.

Melgardt M. de Villiers is a Professor at the University of Wisconsin School of Pharmacy. His current research is focused on determining the pharmaceutical science involved in developing an understanding of the pharmaceutics, engineering, and materials sciences principles underlying enhanced drug delivery technologies. Several of his publications have been related to layer-by-layer nanocoating and to solid-state nanoparticle properties of drugs and excipients. Dr. De Villiers is the associate editor of *AAPS PharmSciTech,* an AAPS fellow and the recipient of the Outstanding Professor in the College of Health Sciences at the University of Louisiana at Monroe.